

1 **Postnatal mechanical loading drives adaptation of tissues primarily through modulation**  
2 **of the non-collagenous matrix**

3

4 D. E. Zamboulis<sup>1</sup>, C. T. Thorpe<sup>2</sup>, Y. Ashraf Kharaz<sup>1</sup>, H. L. Birch<sup>3</sup>, H. R. C. Screen<sup>4</sup>, P. D.  
5 Clegg<sup>1</sup>

6

7 <sup>1</sup>Institute of Ageing and Chronic Disease, Faculty of Health and Life Sciences, University of  
8 Liverpool, Liverpool, L7 8TX, United Kingdom

9 <sup>2</sup>Comparative Biomedical Sciences, The Royal Veterinary College, Royal College Street,  
10 London, NW1 0TU, United Kingdom

11 <sup>3</sup>University College London, Department of Orthopaedics and Musculoskeletal Science,  
12 Stanmore Campus, Royal National Orthopaedic Hospital, Stanmore, HA7 4LP, United  
13 Kingdom

14 <sup>4</sup>Institute of Bioengineering, School of Engineering and Materials Science, Queen Mary  
15 University of London, London, E1 4NS, United Kingdom

16

17

18 **Abstract**

19 Mature connective tissues demonstrate highly specialised properties, remarkably adapted to  
20 meet their functional requirements. Tissue adaptation to environmental cues can occur  
21 throughout life and poor adaptation commonly results in injury. However, the temporal  
22 nature and drivers of functional adaptation remain undefined. Here, we explore functional  
23 adaptation and specialisation of mechanically loaded tissues using tendon; a simple aligned  
24 biological composite, in which the collagen (fascicle) and surrounding predominantly non-  
25 collagenous matrix (interfascicular matrix) can be interrogated independently. Using an

26 equine model of late development, we report the first phase-specific analysis of  
27 biomechanical, structural and compositional changes seen in functional adaptation,  
28 demonstrating adaptation occurs postnatally, following mechanical loading, and is almost  
29 exclusively localised to the non-collagenous interfascicular matrix. These novel data redefine  
30 adaptation in connective tissue, highlighting the fundamental importance of non-collagenous  
31 matrix and suggesting that regenerative medicine strategies should change focus from the  
32 fibrous to the non-collagenous matrix of tissue.

33

### 34 **Introduction**

35 Functional adaptation of load-bearing tissues such as tendon is crucial to ensure the tissue is  
36 specialised appropriately to meet functional needs. Adaptation to mechanical requirements is  
37 key in healthy development and homeostatic tissue maintenance, with poor tissue  
38 optimisation during maturation likely a key contributor to increased injury risk later in life.  
39 Dysregulated homeostasis and long-term under- or over-stimulation leads to maladaptation,  
40 changes in tissue integrity, and reduced mechanical competence and is implicated in the  
41 disease aetiology of load-bearing tissues (Freedman et al., 2015; Gardner et al., 2008).  
42 Understanding the developmental drivers of structural specialisation and their association  
43 with mechanobiology is thus of fundamental importance for healthy ageing and disease  
44 prevention in musculoskeletal tissues (Choi et al., 2018; Thorpe et al., 2013). Such  
45 knowledge will help identify future targets for therapeutic interventions, and thus address the  
46 current lack of effective musculoskeletal disease treatments with new, evidence-based  
47 approaches to disease management. However, there is currently little knowledge of the key  
48 extracellular matrix (ECM) components associated with structural specialisation, the  
49 temporal nature of their adaptation, or the stimuli that drive adaptation.

50 As the principal structural component of connective tissues, collagen expression at the gene

51 and protein level has been the focus of the majority of studies in relation to loading, with  
52 some studies reporting increases in collagen synthesis and others noting collagen degradation  
53 in response to loading, depending on the tissue function or tissue structure in different species  
54 (Choi et al., 2018; Magnusson & Kjaer, 2019). In tendons, this collagen structural framework  
55 is the fascicles and it is surrounded by the primarily non-collagenous and glycoprotein-rich  
56 components of the ECM, termed the interfascicular matrix (IFM) (Figure 1 – Figure  
57 supplement 1b) (Armiento et al., 2018; Thorpe & Screen, 2016). This distinction is important,  
58 as it describes a fibre composite material, in which “fascicle” and “IFM” phases have  
59 different mechanical properties, and overall tissue mechanical properties and function are  
60 governed by the interplay of these two phases. When looking to understand functional  
61 adaption of a tissue, it is necessary to look at adaption of all ECM components.

62 Whilst fascicle and collagen adaptation has received some attention, adaptation of the IFM  
63 phase to mechanical stimuli remains poorly defined. Indeed, it is notable that the numerous  
64 studies investigating the mechanoresponsive nature of load-bearing tissues tend to restrict  
65 their focus to specific fibre or matrix components with no spatial distinction, and also focus  
66 on a single element of either structural or mechanical adaptation, such that limited  
67 information is gained (Cherdchutham, Becker, et al., 2001; Choi et al., 2019; Mendias et al.,  
68 2012). In order to provide the necessary complete profile of adaptive behaviour, it is crucial  
69 that phase-specific, temporospatial adaptation in the context of both structure and function is  
70 defined.

71 Identifying the drivers of adaptation requires use of a model system in which the  
72 temporospatial nature of adaptation can be fully profiled. Tendon provides the ideal model  
73 for such a study. It is well-established that mature tendons can present structural and  
74 mechanical specialisms (Thorpe, Godinho, et al., 2015; Thorpe, Karunaseelan, et al., 2016;  
75 Thorpe, Riley, et al., 2016) and be grouped into two clear functional groups; stiff positional

76 tendons, such as the anterior tibialis tendon and the equine common digital extensor tendon  
77 (CDET), that simply connect muscle to bone to effectively position limbs, whilst elastic  
78 energy-storing tendons, such as the Achilles tendon and the equine superficial digital flexor  
79 tendon (SDFT), are further specialised to provide an energy storing function, increasing  
80 locomotor efficiency by stretching and storing energy which they return to the system on  
81 recoil (Alexander, 2002; Batson et al., 2003; Thorpe et al., 2012; Thorpe & Screen, 2016).  
82 Further, the simple aligned organisation of tendon means that fascicle and IFM phases are  
83 spatially distinct, enabling structural and mechanical characterisation of each phase  
84 independently (Thorpe et al., 2012; Thorpe & Screen, 2016). Finally, use of equine tendon  
85 provides access to an exceptional model of adaptation. The SDFT has been shown to be  
86 highly analogous to the human Achilles tendon in its capacity for energy storage, injury  
87 profile and extent of specialization and the anatomically opposing CDET is an example of a  
88 positional tendon, functionally comparable to the human anterior tibialis tendon (Figure 1 –  
89 Figure supplement 1a) (Biewener, 1998; Patterson-Kane & Rich, 2014). Availability of  
90 samples enabled us to explore the extensive adaptation processes associated with late stage  
91 development, contrasting paired positional and energy-storing equine tendons through pre-  
92 and post-natal development.

93 Using this model, we investigate the process and drivers of functional adaptation, when  
94 tendons transition from an absence of loading (foetal: mid to end (6 to 9 months) gestation,  
95 and 0 days: full-term foetuses, and foals that did not weight-bear); through to weight-bearing  
96 (0-1 month) and then to an increase in body weight and physical activity (3-6 months; and 1-  
97 2 years). We hypothesise that early in development during gestation, the fascicle and IFM of  
98 functionally distinct tendons have identical compositional profiles and mechanical properties,  
99 with tissue specialisation occurring as an adaptive response to the mechanical stimulus of  
100 load-bearing, predominantly in the IFM of the elastic energy-storing tendon.



101

## 102 **Results**

### 103 **Mechanical adaptation is localised to the IFM**

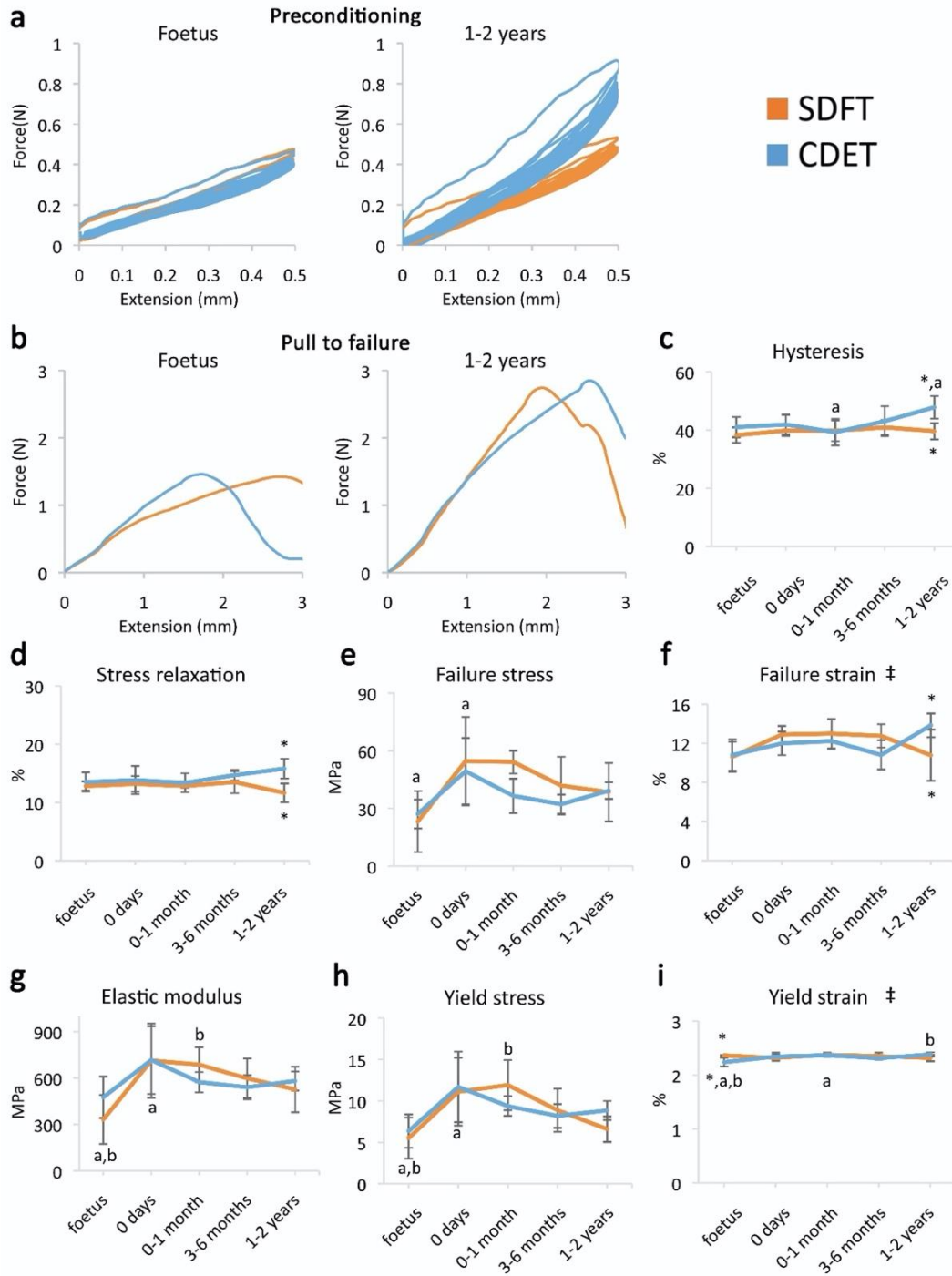
104 First, we determined how the mechanical properties of the fascicle and IFM develop in  
105 tendon, with a particular focus on the temporospatial nature of mechanical adaptation and  
106 functional specialisation. Individual fascicles were dissected while an isolated region of IFM  
107 was tested by shearing fascicles apart (Figure 1 – Figure supplement 1c). Samples were  
108 subjected to preconditioning followed by a pull to failure (Figure 1 – Figure supplement 1c).  
109 The yield point of samples was identified, denoting the point at which the sample became  
110 irreversibly damaged and was unable to recover from the applied load, and the sample failure  
111 properties also recorded, highlighting the maximum stress and strain the sample could  
112 withstand.

113 A significant increase in fascicle yield and failure properties was evident when comparing  
114 embryonic fascicles to those acquired immediately at birth (Figure 1h-i and 1e-g,  
115 respectively). However, data indicate minimal distinction in fascicle mechanics between  
116 functionally distinct tendons (Figure 1e-i) and, significantly, no specialisation for energy  
117 storage in response to loading during postnatal development.

118 Contrasting with fascicle mechanics, the failure properties of the IFM continued to alter  
119 throughout development with failure properties increasing markedly from 6 months onwards  
120 (Figure 2e-g). We also identify the emergence of an extended region of low stiffness at the  
121 start of the loading curve (ie an extended toe region) specific to the SDFT IFM pull to failure  
122 curve (Figure 2b). This indicates less resistance to extension, and together with the  
123 concomitant increase in IFM yield force and extension at yield (Figure 2h-i), demonstrates  
124 development of an overall greater capacity for extension in the SDFT IFM behaviour. A

125 summary of these findings is achieved by plotting the amount of IFM extension at different  
126 percentages of failure force (Figure 2j-k), highlighting how the IFM of the energy-storing  
127 SDFT became significantly less stiff than that of the positional CDET during the initial toe  
128 region of the loading curve as the tendon adapts.

129 The viscoelastic properties of the developing IFM also showed significant interactions  
130 between tendon type and development, with IFM viscoelasticity significantly decreasing with  
131 development specifically in the energy-storing SDFT (Figure 2a, c-d), resulting in  
132 specialisation towards a more energy efficient structure.

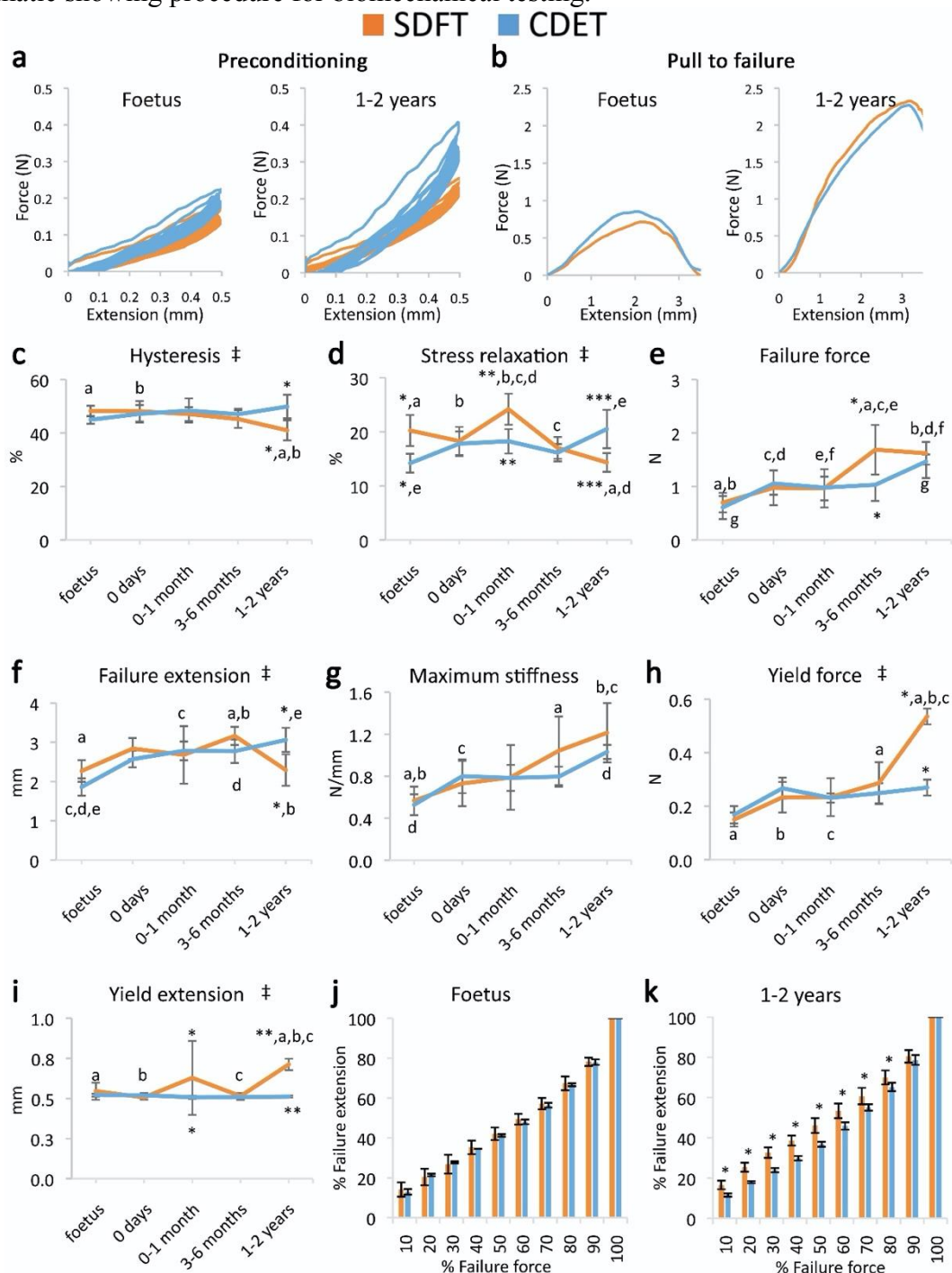


134

135 **Figure 1. Fascicle response to mechanical testing shows increase in strength with**  
 136 **development but few significant differences between tendon types, indicating that the**  
 137 **fascicles show minimal structural specialisation in response to loading. (a)**

138 Representative curves for 10 preconditioning cycles for the SDFT and CDET fascicles in the  
 139 foetus and 1-2 years age group. (b) Representative force-extension curves to failure for the  
 140 SDFT and CDET fascicles in the same age groups. (c-i) Mean SDFT and CDET fascicle  
 141 biomechanical properties are presented across development, with data grouped into age  
 142 groups: foetus, 0 days (did not weight-bear), 0-1 month, 3-6 months, 1-2 years. ‡ significant  
 143 interaction between tendon type and development, \* significant difference between tendons,  
 144 a-b significant difference between age groups. Error bars depict standard deviation. **Figure 1**

145 – **Figure supplement 1.** SDFT and CDET in the equine forelimb, tendon structure, and  
 146 schematic showing procedure for biomechanical testing.



147

148 **Figure 2. Mechanical testing of the IFM shows an equivalent increase in failure**  
 149 **properties between the SDFT and CDET with development, but development of an**  
 150 **extended low stiffness toe region and more elastic behaviour in the SDFT. (a)**  
 151 **Representative curves for 10 preconditioning cycles for the SDFT and CDET IFM in the**  
 152 **foetus and 1-2 years age group. (b) Representative force-extension curves to failure for the**  
 153 **SDFT and CDET IFM in the same age groups. (c-i) Mean SDFT and CDET IFM**  
 154 **biomechanical properties are presented across development, with data grouped into age**  
 155 **groups: foetus, 0 days (did not weight-bear), 0-1 month, 3-6 months, 1-2 years. (j-k) To**  
 156 **visualise the extended low stiffness toe region in the SDFT IFM, the amount of IFM**

157 extension at increasing percentages of failure force is presented, comparing the SDFT and  
158 CDET in the foetus and 1-2 years age group. ‡ significant interaction between tendon type  
159 and development, \* significant difference between tendons, a-g significant difference  
160 between age groups. Error bars depict standard deviation.  
161

## 162 **Structural adaptation is localised to the IFM**

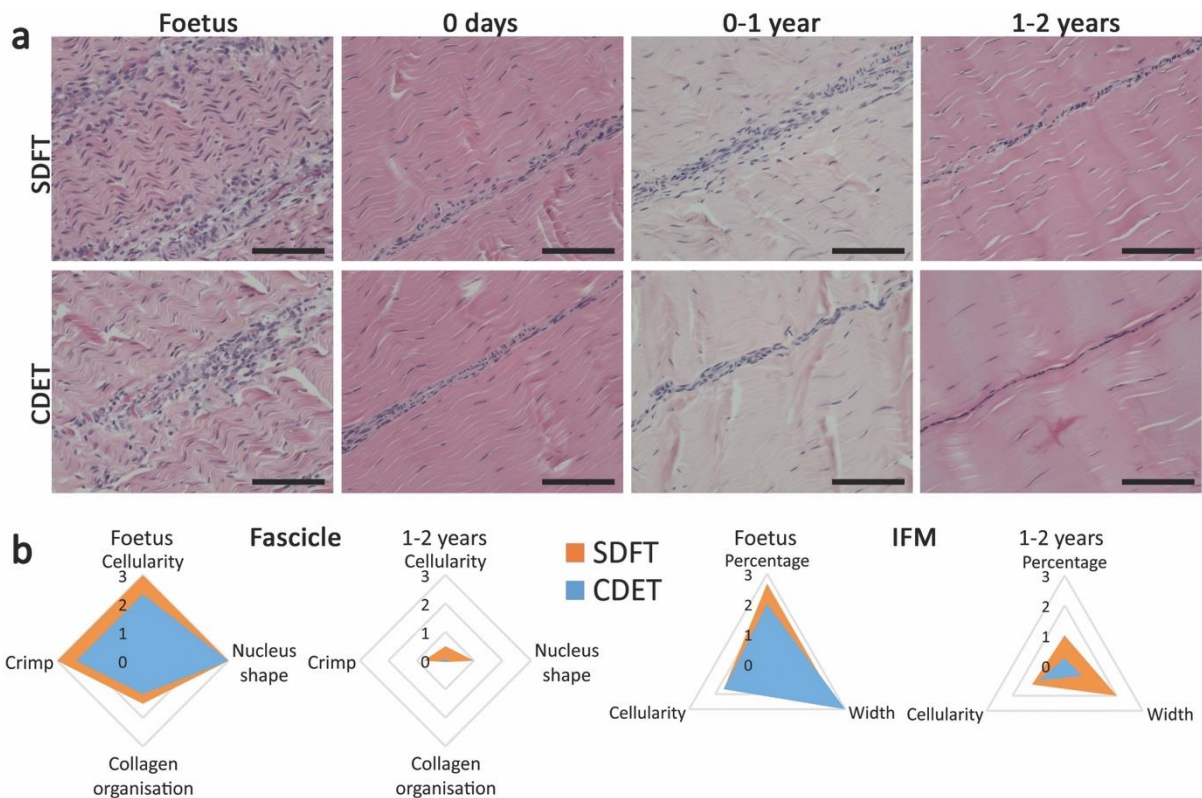
163 Having described the mechanical adaptation of the IFM to meet functional demand, we next  
164 performed a histological and immunohistochemical comparison of developing energy-storing  
165 and positional tendons to determine how temporospatial structural adaptation may dictate this  
166 evolving mechanical behaviour.

167 The energy-storing SDFT and positional CDET appeared histologically similar in the foetus,  
168 in both instances showing surprisingly poor demarcation of the IFM, which only became  
169 structurally distinct after birth and the initiation of loading (Figure 3a). Fascicle development  
170 was generally consistent in both tendon types with cellularity and crimp showing a reduction  
171 with development, cells displaying more elongated nuclei, and collagen showing a more  
172 linear organisation (Figure 3b, Figure 3 – Figure supplement 1, scoring criteria  
173 Supplementary File 1). In contrast, the IFM demonstrated divergence between tendon types  
174 with only the SDFT IFM showing an increase in cellularity following tendon loading and a  
175 retention of IFM width throughout development (Figure 3b, Figure 3 – Figure supplement 1).

176 The abundance of major ECM proteins was also generally consistent across fascicle and IFM  
177 in the foetus, with divergence of protein composition between phases only evident with  
178 further development (Figure 4). Notably adaptation was driven by changes in non-  
179 collagenous ECM components specifically, levels of which reduced in the fascicles and  
180 increased dramatically in the IFM through postnatal development (Figure 4, Figure 4 – Figure  
181 supplement 1). Of particular note, we demonstrate PRG4 (commonly known as lubricin) and  
182 TNC were predominantly found in the IFM of tendons and showed sparse staining or were  
183 absent, respectively, from the fascicles. We also demonstrate that elastin is preferentially

184 localised to the IFM with its abundance decreasing only in the CDET with development.  
 185 Furthermore, we show histological and compositional changes manifest after birth and with  
 186 the initiation of loading, but that histological and compositional adaptation to loading then  
 187 occurs over a period of months, involving both upregulation and downregulation of different  
 188 histologic variables and ECM constituents.

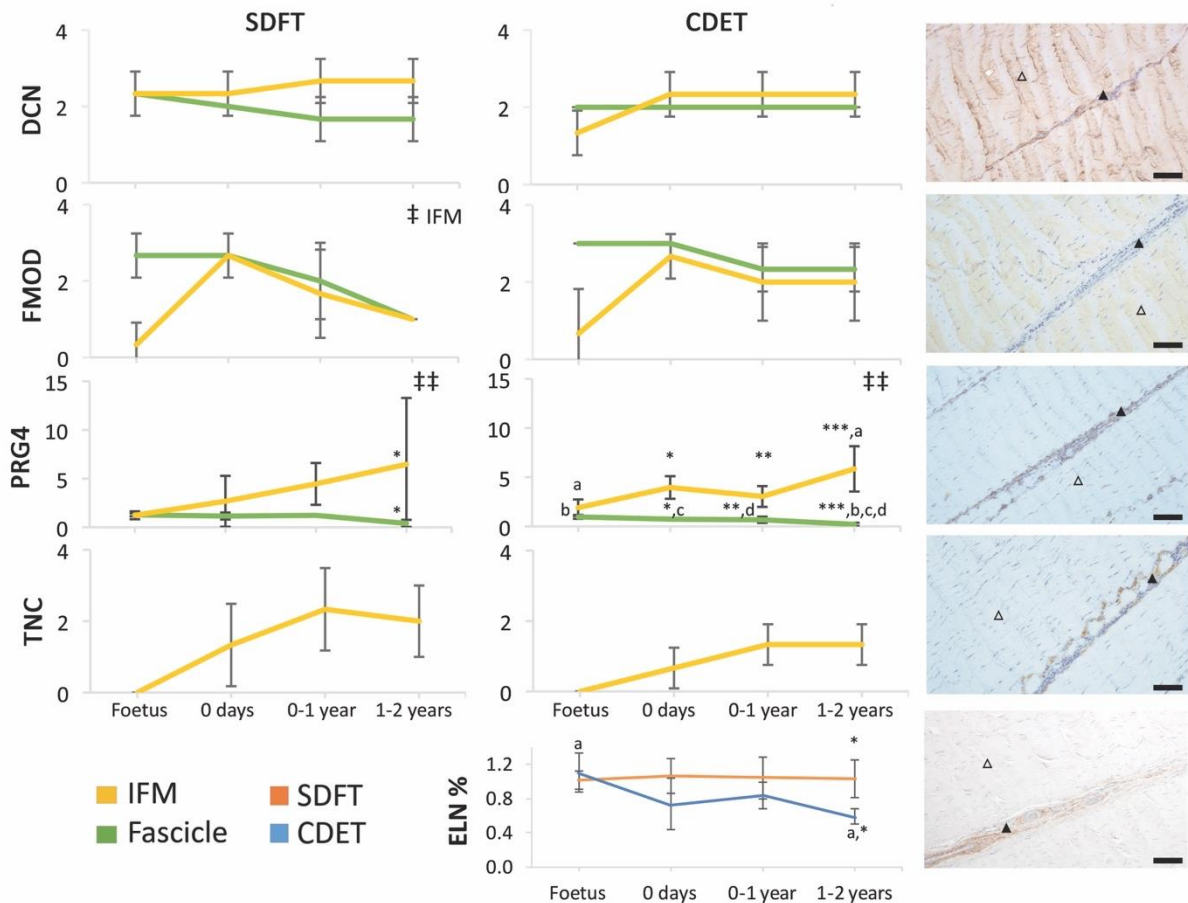
189



190

191 **Figure 3. The SDFT and CDET are histologically similar at birth and differentiate with**  
 192 **development especially in the IFM.** (a) Representative images of H&E sections of the  
 193 SDFT and CDET demonstrate structural development: foetus, 0 days (did not weight-bear),  
 194 0-1 year, and 1-2 years whilst (b) Radar plots enable the mean histology scores of the fascicle  
 195 and IFM for the SDFT and CDET to be compared between the foetus and 1-2 years age  
 196 group (all data shown in Figure 3 – Figure supplement 1 and scoring criteria in  
 197 Supplementary File 1). A decrease in cell numbers, crimp, and IFM width is visible with  
 198 progression of age, and the aspect ratio of cells in the fascicle increases. Scale bar 100  $\mu$ m.  
 199 **Figure 3 – Figure supplement 1.** Scoring of histologic variables for the IFM and fascicle in  
 200 the SDFT and CDET through postnatal development.  
 201





202

203 **Figure 4. Immunohistochemical assays show divergence of PGR4 (lubricin) and elastin**  
 204 **with maturation between functionally distinct tendons.** IFM and fascicle staining scores  
 205 are shown for decorin (DCN), fibromodulin (FMOD), lubricin (PRG4), and tenascin-C  
 206 (TNC) in the SDFT and CDET, alongside representative images of immunohistochemical  
 207 staining in the postnatal SDFT. DCN and FMOD staining is found in both IFM (black  
 208 triangle) and fascicle (white triangle). PRG4 staining is mainly located in the IFM (black  
 209 triangle) and less staining can be found in the fascicle (white triangle). TNC staining is  
 210 restricted to the IFM (black triangle) and absent from the fascicle (white triangle). A  
 211 quantitative measure of elastin (ELN) is provided as percentage of wet weight, alongside a  
 212 representative image of immunohistochemical staining in the postnatal SDFT. ELN staining  
 213 is mainly located in the IFM (black triangle) and faint staining can be found in the fascicle  
 214 (white triangle). Staining scores for elastin are provided in Figure 4 – Figure supplement 1. ‡  
 215 significant change in tendon phase with development, ‡‡ significant interaction between  
 216 tendon phase and development, \* significant difference between tendons, a-d significant  
 217 difference between age groups. Scale bar 100 μm. Error bars depict standard deviation.  
 218 **Figure 4 – Figure supplement 1.** Scoring of ELN staining for the IFM and fascicle in the  
 219 SDFT and CDET through postnatal development.

220

221

222

223

## 224 **Adaptation relies on evolution of IFM composition only**

225 To explore these concepts in further detail and to scrutinise the capacity for ECM adaptation,  
226 proteomic methodologies were adopted. With the mechanical and histological data  
227 identifying that functional adaptation is particular to the energy-storing SDFT, mass  
228 spectrometry analysis focused on a more detailed comparison of the IFM and fascicle  
229 development and adaptation in this tendon specifically.

230 Our results demonstrated that the proteomic profile of the IFM was more complex (more  
231 identified proteins) and a higher percentage of IFM proteins were cellular (Figure 5 – Figure  
232 supplement 1), supporting the histological findings of a more cellular IFM. Notably, despite  
233 the two phases being structurally distinct, they had 14 collagens and 11 proteoglycans in  
234 common (Supplementary File 4). Overall, proteomic heatmap analysis correlated very  
235 strongly with immunohistochemical findings, showing that alterations in the fascicle  
236 proteome reduced through development, with minimal changes following the initiation of  
237 loading (Table 1 and 2, Figure 5a), whilst numerous matrisome and matrisome-related  
238 proteins progressively increase in abundance through development in the IFM (Table 1 and 2,  
239 Figure 5a). Detailed consideration of protein changes also highlights that post loading  
240 changes in the IFM appear more specific to proteoglycans and glycoproteins. Correlation  
241 analysis of IFM matrisome protein abundance and mechanical properties of the IFM across  
242 development revealed correlations for matrisome proteins abundance with the mechanical  
243 properties correlating IFM ECM composition and functional adaptation. Significant  
244 correlations included a negative correlation between proteoglycans DCN, LUM, OGN,  
245 PRELP and COL3A1 and the IFM hysteresis, a positive correlation between FBLN5 and  
246 stress relaxation, a positive correlation between COL6A1, COL6A2, and OGN and maximum  
247 stiffness, and for the yield properties a positive correlation of proteoglycans DCN, LUM,  
248 OGN, PRELP and COL3A1 and force at yield point (Supplementary File 5). In addition,



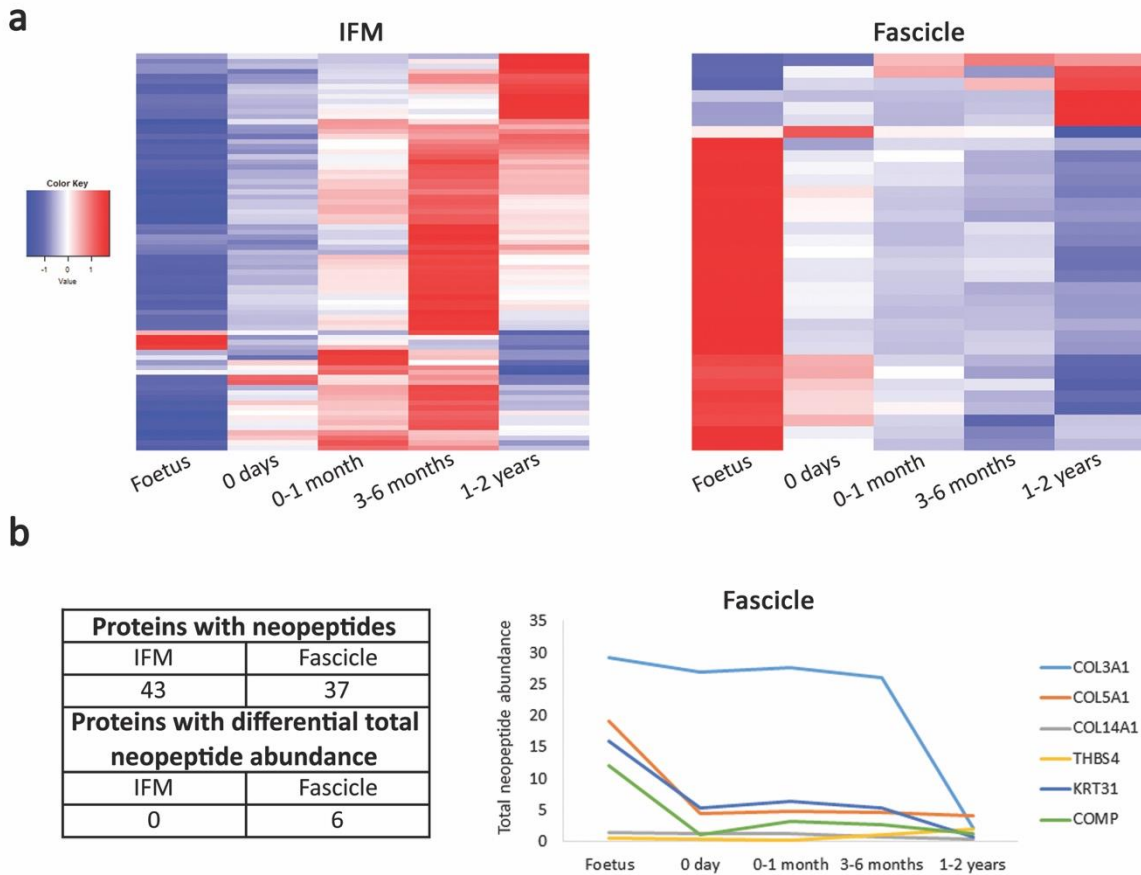
249 protein abundance for BGN, DCN, COMP, COL1A2, COL3A1 in the IFM and COMP and  
250 COL3A1 in the fascicles across development is mirrored by whole tendon mRNA expression  
251 (Figure 5 – Figure supplement 2).

252 Proteomic data also enabled insight into the turnover of proteins in the different tendon  
253 phases, through a comparison of the neopeptides produced by protein breakdown (Thorpe,  
254 Peffers, et al., 2016). In the current study, we were able to profile the temporal nature of  
255 fascicle and IFM turnover, demonstrating that both phases display turnover during  
256 development but that fascicle turnover slows down towards the end of maturation, whilst IFM  
257 turnover rates are maintained, suggesting structural and/or compositional plasticity (Figure  
258 5b).

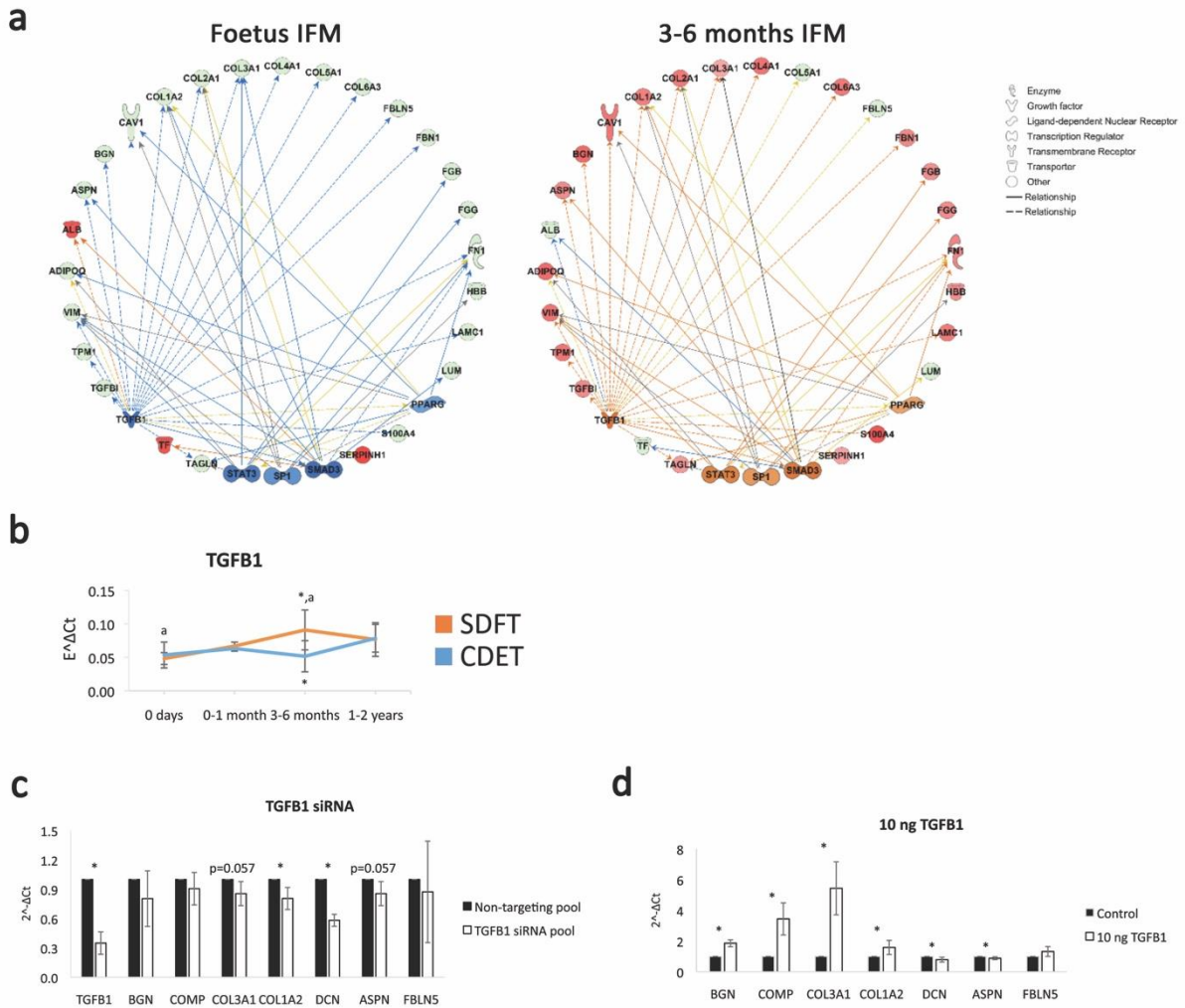
259 Having identified the IFM as the location of functional adaptation, we next investigated the  
260 regulation of this process, to detect targets for modulation for regeneration strategies  
261 addressing functional impairment. For this purpose, pathway analysis was carried out for the  
262 differentially abundant proteins identified with mass spectrometry across age groups using  
263 the Ingenuity Pathway Analysis software (IPA). Pathway analysis revealed the canonical  
264 pathways “integrin signaling” and “actin cytoskeleton signaling” were predicted to be  
265 activated with development in the IFM supporting an ECM-integrin-cytoskeleton to nucleus  
266 signalling pathway for the mediation of the observed mitogenesis and matrigenesis in  
267 response to tendon loading. In addition, pathway analysis identified TGFB1 as an upstream  
268 regulator for the IFM dataset and based on the IFM protein abundance across age groups  
269 predicted TGFB1 to be inhibited in the foetus age group and to become activated in the 3-6  
270 months age group. TGF- $\beta$ 1 was therefore highlighted as a potential regulator of ECM  
271 organisation and functional adaptation, predicted to be upregulated in the energy-storing  
272 tendon following loading (Figure 6a). This was supported by TGB1 mRNA expression in  
273 whole tendon increasing in the 3-6 months SDFT only, with the positional CDET TGFB1

274 expression showing no change with development (Figure 6b). In addition, knockdown of  
275 TGFB1 in equine adult tenocytes and stimulation with 10 ng recombinant TGF- $\beta$ 1 showed  
276 downregulation and upregulation, respectively, of key ECM components, BGN, COMP,  
277 COL1A2, and COL3A1, supporting a regulatory role for TGF- $\beta$ 1 (Figure 6c-d). Finally,  
278 correlation analysis of TGFB1 mRNA expression of whole tendon and IFM matrixome  
279 protein abundance across development revealed positive correlations with ECM proteins  
280 which were significant for COL1A2, COL2A1, COL4A1, COL4A2, COL6A3, HSPG2, and  
281 FN1 (Supplementary File 6).

282



































283  
 284 **Figure 5. The fascicle proteome remains the same during postnatal development and**  
 285 **tendon loading whereas the IFM proteome starts changing following tendon loading in**  
 286 **postnatal development.** (a) Heatmap of differentially abundant proteins in foetus, 0 days  
 287 (did not weight-bear), 0-1 month, 3-6 months, and 1-2 years SDFT IFM and fascicles  
 288 ( $p < 0.05$ , fold change  $\geq 2$ ). Heatmap colour scale ranges from blue to white to red with blue  
 289 representing lower abundance and red higher abundance. (b) Proteins with identified  
 290 neopeptides and proteins showing differential total neopeptide abundance across age groups.  
 291 Graph of proteins showing differential total neopeptide abundance in the SDFT fascicles  
 292 across development ( $p < 0.05$ , fold change  $\geq 2$ , FDR 5%). No proteins showed differential total  
 293 neopeptide abundance in the IFM. **Figure 5 – Figure supplement 1.** Classification of SDFT  
 294 IFM and fascicle identified proteins and differentially abundant proteins according to their  
 295 associated location. **Figure 5 – Figure supplement 2.** Relative mRNA expression of major  
 296 ECM genes in whole tissue SDFT and CDET through postnatal development.  
 297  
 298



299  
 300  
 301  
 302  
 303  
 304  
 305  
 306  
 307  
 308  
 309  
 310  
 311  
 312  
 313  
 314

**Figure 6. TGFβ1 is predicted to be involved in compositional changes observed in the IFM.** (a) IPA networks for TGFβ1 as an upstream regulator were generated for the foetus and 3-6 months SDFT IFM proteomic datasets. TGFβ1 regulation in the IFM is predicted to be inhibited in the foetus and activated at 3-6 months in the SDFT. Red nodes, upregulated proteins, green nodes, downregulated proteins, intensity of colour is related to higher fold-change, orange nodes, predicted upregulated proteins in the dataset, blue nodes, predicted downregulated proteins. (b) Whole tendon relative mRNA expression for TGFβ1 in the SDFT and CDET during postnatal development shows an increase in TGFβ1 mRNA in the 3-6 months highly-loaded SDFT only. \* significant difference between tendons, a significant difference between age groups. (c-d) Relative mRNA expression of major ECM genes predicted to be regulated by TGFβ1 in the IPA network following TGFβ1 knockdown (c) and stimulation with 10 ng recombinant TGF-β1 (d) for 24 hours. BGN, DCN, COMP, COL1A2 and COL3A1 show regulation following TGFβ1 knockdown or addition. \* significant difference between control and treatment. Error bars depict standard deviation.

315 **Table 1. IFM differentially abundant matrisome and matrisome-associated proteins**  
 316 **through development organised by highest mean condition ( $p < 0.05$ , fold change  $\geq 2$ ).**  
 317 Proteins are arranged into colour coded divisions and categories. Bar graphs profile the  
 318 relative abundance of each protein at each development stage, a foetus, b 0 days, c 0-1 month,  
 319 d 3-6 months, e 1-2 years, with the development age reporting the highest mean protein level  
 320 also specified.
















Protein	Division	Category	Highest mean cond.	a b c d e
SERPINH1	Matrisome-associated	ECM Regulators	Foetus	
COL14A1	Core matrisome	Collagens	0-1 month	
ASPN	Core matrisome	Proteoglycans	0-1 month	
FMOD	Core matrisome	Proteoglycans	0-1 month	
KERA	Core matrisome	Proteoglycans	0-1 month	
FBLN5	Core matrisome	ECM Glycoproteins	0-1 month	
FGB	Core matrisome	ECM Glycoproteins	0-1 month	
FGG	Core matrisome	ECM Glycoproteins	0-1 month	
COL1A2	Core matrisome	Collagens	3-6 months	
COL2A1	Core matrisome	Collagens	3-6 months	
COL4A1	Core matrisome	Collagens	3-6 months	
COL4A2	Core matrisome	Collagens	3-6 months	
COL6A3	Core matrisome	Collagens	3-6 months	
BGN	Core matrisome	Proteoglycans	3-6 months	
HSPG2	Core matrisome	Proteoglycans	3-6 months	
ADIPOQ	Core matrisome	ECM Glycoproteins	3-6 months	
FBN1	Core matrisome	ECM Glycoproteins	3-6 months	
FN1	Core matrisome	ECM Glycoproteins	3-6 months	
LAMB2	Core matrisome	ECM Glycoproteins	3-6 months	
LAMC1	Core matrisome	ECM Glycoproteins	3-6 months	
NID1	Core matrisome	ECM Glycoproteins	3-6 months	
ANXA4	Matrisome-associated	ECM-affiliated	3-6 months	
S100A4	Matrisome-associated	Secreted Factors	3-6 months	
COL21A1	Core matrisome	Collagens	1-2 years	
COL3A1	Core matrisome	Collagens	1-2 years	
COL5A1	Core matrisome	Collagens	1-2 years	
COL5A2	Core matrisome	Collagens	1-2 years	
COL6A1	Core matrisome	Collagens	1-2 years	
COL6A2	Core matrisome	Collagens	1-2 years	
DCN	Core matrisome	Proteoglycans	1-2 years	
LUM	Core matrisome	Proteoglycans	1-2 years	
OGN	Core matrisome	Proteoglycans	1-2 years	
PRELP	Core matrisome	Proteoglycans	1-2 years	
COMP	Core matrisome	ECM Glycoproteins	1-2 years	
DPT	Core matrisome	ECM Glycoproteins	1-2 years	

TGFBI	Core matrisome	ECM Glycoproteins	1-2 years	
-------	----------------	-------------------	-----------	---

321

322 **Table 2. Fascicle differentially abundant matrisome and matrisome-associated proteins**  
 323 **through development organised by highest mean condition ( $p < 0.05$ , fold change  $\geq 2$ ).**

324 Proteins are arranged into colour coded divisions and categories. Bar graphs on the right  
 325 profile the relative abundance of each protein at each development stage, a foetus, b 0 days, c  
 326 0-1 month, d 3-6 months, e 1-2 years, with the development age reporting the highest mean  
 327 protein level also specified.

Protein	Division	Category	Highest mean cond.	a b c d e
COL11A1	Core matrisome	Collagens	Foetus	
DCN	Core matrisome	Proteoglycans	Foetus	
FMOD	Core matrisome	Proteoglycans	Foetus	
KERA	Core matrisome	Proteoglycans	Foetus	
PCOLCE	Core matrisome	ECM Glycoproteins	Foetus	
SERPINF1	Matrisome-associated	ECM Regulators	Foetus	
ANXA1	Matrisome-associated	ECM-affiliated Proteins	Foetus	
ANXA2	Matrisome-associated	ECM-affiliated Proteins	Foetus	
ANXA5	Matrisome-associated	ECM-affiliated Proteins	Foetus	
LGALS1	Matrisome-associated	ECM-affiliated Proteins	Foetus	
COL12A1	Core matrisome	Collagens	0 days	
COL3A1	Core matrisome	Collagens	1-2 years	
PRELP	Core matrisome	Proteoglycans	1-2 years	
COMP	Core matrisome	ECM Glycoproteins	1-2 years	
FN1	Core matrisome	ECM Glycoproteins	1-2 years	

328

329

### 330 Discussion

331 In this study, we describe the phase-specific process and drivers of functional adaptation in  
 332 tendon development integrating mechanical, structural, and compositional analysis in tendons  
 333 transitioning from an absence of loading through to weight-bearing and then to an increase in  
 334 body weight and physical activity. To investigate functional adaptation and structure-function  
 335 specialisation, we are contrasting fascicles and IFM of two tendons with distinct functions  
 336 and mechanical properties; the equine SDFT and CDET. The energy-storing SDFT, which

337 functions by stretching and recoiling with each stride to store and return energy, undergoes  
338 peaks strains recorded at 16.6 % *in vivo* and has been found to be significantly more  
339 extensible than the CDET. The positional CDET, which functions to extend the distal limb  
340 prior to limb placement and is relatively inextensible to allow precise placement of the limb,  
341 experiences much lower strains than the SDFT (estimated at 2.5 %) and is less extensible  
342 than the SDFT (Batson et al., 2003; Birch et al., 2008; Thorpe et al., 2012).

343 Whilst the limited previously available data on the development of tendon gross mechanical  
344 properties show an increase in mechanical properties with development (Ansorge et al., 2011;  
345 Cherdchutham, Meershoek, et al., 2001), no such phase-specific analysis of the development  
346 of tissue mechanics has been carried out previously. Similarly, available research into tendon  
347 morphogenesis and maturation has previously focused on the development of the collagenous  
348 network that comprises the tendon fascicles and is often focussed on early foetal development  
349 (Kalson et al., 2011; Marturano et al., 2013; Pan et al., 2018). Murine and zebrafish models  
350 used to investigate tendon development and adaptation have advanced our understanding of  
351 the control of fibrillogenesis by ECM proteins (Subramanian et al., 2018; Subramanian &  
352 Schilling, 2014; Taye et al., 2020) but these models lack an IFM, thus restricting our ability  
353 to explore the functional specialism we see in humans and other larger mammals.

354 Here, examining the fascicle and IFM mechanical properties independently, we show  
355 minimal distinction in fascicle mechanics between functionally distinct tendons and,  
356 significantly, no specialisation for energy storage in response to loading during postnatal  
357 development. In contrast, the IFM mechanical properties display continuous alterations  
358 through development with the properties of the IFM in the foetus being comparable between  
359 functionally distinct tendons, and a low stiffness region emerging in the initial non-linear  
360 region (toe region) of the pull to failure curve of the SDFT IFM only following tendon  
361 loading postnatally. This is coupled with a concomitant increase in IFM force and extension

362 at yield, the point at which the sample became irreversibly damaged, highlighting that the  
363 energy-storing SDFT IFM becomes significantly less stiff than that of the positional CDET  
364 during the initial toe region of the loading curve. We have previously indicated that this low  
365 stiffness behaviour allows sliding between the fascicles, enabling non-uniform loading of  
366 tissue and is fundamental for effective extension and recoil in energy-storing tendons  
367 (Thorpe, Godinho, et al., 2015). Furthermore, with ageing the low stiffness behaviour of the  
368 energy-storing IFM is lost, possibly contributing to disease development (Thorpe et al.,  
369 2013). The only other studies considering the mechanical properties of developing tendons  
370 have focused simply on changes in whole tissue mechanics, and have thus not been able to  
371 identify the drivers of change within the tissue (Ansorge et al., 2011; Cherdchutham,  
372 Meershoek, et al., 2001). Here, we identify that the IFM is the key region in which  
373 mechanical adaptation to meet function occurs, and that this occurs after the initiation of  
374 loading, primarily 1-2 years postnatally.

375 We subsequently examine how temporospatial structural adaptation may dictate this evolving  
376 mechanical behaviour and uncover a divergence in structural characteristics between tendon  
377 types in the IFM only, with a retention of IFM width throughout development and an increase  
378 in cellularity in the SDFT IFM only. It is well recognised that foetal and early postnatal  
379 tendons are highly cellular, and cellularity is generally considered to decrease postnatally  
380 (Russo et al., 2015; Stanley et al., 2008), but here we show that the described reduction in  
381 cellularity only occurs in the fascicles, and cellularity in fact increases in the IFM with  
382 development. By following the alterations in cellularity across IFM and fascicle, here we can  
383 determine that the marked difference in regional cellularity is likely driven by a maintenance  
384 of cell numbers following tendon loading in the thinning IFM, while cell numbers in the  
385 fascicle appear to reduce as a result of the fascicle ECM increase. Greater cellularity is  
386 commonly associated with a requirement for rapid adaptive organisation of ECM components



387 (Russo et al., 2015), suggesting the IFM, particularly in the energy-storing tendons, may  
388 adapt to be more mechanoresponsive, a necessary aspect of healthy homeostatic maintenance  
389 of a tissue. Immunohistochemical analysis reveals the distribution of major ECM proteins is  
390 consistent across tendons in the foetus and becomes distinct across compartments through  
391 development. Of note, PRG4 (lubricin), a large proteoglycan which is important in ECM  
392 lubrication, is found mainly distributed in the IFM of tendons. Using a lubricin-knockout  
393 mouse, this proteoglycan has been demonstrated to facilitate interfascicular sliding (Kohrs et  
394 al., 2011), indicating that this structural adaptation may be key in achieving the previously  
395 identified mechanical adaptation in the energy-storing tendon IFM. In addition,  
396 Kostrominova and Brooks (2013) (Kostrominova & Brooks, 2013) report PRG4 expression  
397 as well as elastin expression decreased with ageing in rat tendon suggesting an association  
398 with an increased risk of disease with ageing. We also demonstrate that elastin is  
399 preferentially localised to the IFM, potentially having a role in the capacity for matrix recoil  
400 after loading which is necessary for the healthy function of energy-storing tendons (Godinho  
401 et al., 2017; Ritty et al., 2002). Further supporting a role for elastin in the energy-storing  
402 function, elastin appears to be redundant in positional tendons with its abundance decreasing  
403 in the CDET with development. Together, these findings show that structural adaptation of  
404 tendon post loading is primarily focused to the IFM, and observed predominantly in the  
405 energy-storing SDFT.

406 Compositional analysis of the energy-storing SDFT compartments using mass spectrometry  
407 corroborates the immunohistochemical analysis and shows a more complex proteomic profile  
408 for the IFM. It additionally shows that abundance of the majority of proteins in the fascicles  
409 is higher in the foetus and reduces through development with minimal changes following the  
410 initiation of loading, whereas in the IFM numerous ECM and ECM-related proteins  
411 progressively increase in abundance following tendon loading and through development.

412 Neopeptide analysis demonstrated ECM protein turnover in the fascicles slows down towards  
413 the end of maturation, whilst ECM protein turnover rates in the IFM are maintained. Once a  
414 tendon is mature, little collagen turnover occurs (Birch, 2007; Heinemeier et al., 2013) and  
415 we have previously shown that the minimal turnover in mature tendon is focused to the IFM  
416 (Simpson et al., 2020; Thorpe et al., 2010; Thorpe, Chaudhry, et al., 2015; Thorpe, Peffers, et  
417 al., 2016). The maintenance of turnover rates observed in the IFM here suggests structural  
418 and/or compositional plasticity of the IFM. Integrated, our data convincingly show a  
419 continual temporal change in the IFM proteome specifically, which would enable adaptation  
420 and specialisation to the load environment, and highlight the compositional plasticity of the  
421 IFM in responding to dynamic altered conditions such as those occurring during development  
422 and regeneration. It is critical that the difference in capacity for functional adaptation across  
423 IFM and fascicle identified here is considered if regenerative medicine and tissue engineering  
424 approaches are to be successful. Here, we demonstrate the temporal pattern of structure-  
425 function adaptation, with compositional changes occurring in the first months after loading,  
426 and leading to the mechanical specialisation we have previously observed in adult energy-  
427 storing tendon (Birch, 2007; Thorpe et al., 2012; Thorpe, Godinho, et al., 2015). With the  
428 fascicles primarily responsible for the mechanical strength of a tissue, biomaterial and  
429 regenerative medicine studies have unsurprisingly placed considerable emphasis on this  
430 region to date (Sensini et al., 2019; Watts et al., 2017). Here, we not only highlight the  
431 importance of the IFM in modulating mechanical behaviour, but also demonstrate how the  
432 IFM must be targeted to support adaptation and optimum tissue quality.

433 Finally, pathway analysis of our proteomic data highlighted TGF- $\beta$ 1 as a regulator of ECM  
434 organisation and functional adaptation, predicted to be upregulated following loading in the  
435 energy-storing tendon. TGF- $\beta$  is a known regulator of proteoglycans and collagens in tendon  
436 (Potter et al., 2017; Robbins et al., 1997), a role we also demonstrated here with regulation of

437 major ECM proteins mRNA expression following TGFB1 knockdown and stimulation in  
438 equine tenocytes. Further, TGFB1 mRNA expression was upregulated in the highly loaded  
439 energy-storing tendon only, supporting the hypothesis that TGF- $\beta$ 1 regulation is specific to  
440 the energy-storing tendon and subsequently indicating that it may specifically be associated  
441 with loading. Exploring the specificity of TGF- $\beta$ 1 regulation and loading is challenging.  
442 Muscle paralysis interventions can be used to demonstrate a causal effect between  
443 mechanical force and TGF- $\beta$  regulation (Subramanian et al., 2018) however such  
444 experiments cannot be conducted in horses and other large mammals.

445 Whilst we acknowledge that other extrinsic factors may drive the changes, our direct  
446 comparison of the highly loaded SDFT with the low load CDET enables us to identify that  
447 the divergence in mechanical properties, adaptation, and TGF- $\beta$  regulation all occurs only in  
448 the tendon experiencing significant loading. In addition, TGF- $\beta$  has been shown to have a  
449 role in cellular mechanobiology and connective tissue homeostasis, regulating ECM synthesis  
450 and remodelling in a force-dependent way following mechanical stimulation, to specify the  
451 quality of the ECM and help coordinate cytoskeletal tension (Maeda et al., 2011;  
452 Subramanian et al., 2018). A previous study of developing chick tendon detected TGF- $\beta$ 1  
453 staining in the IFM only, during development, highlighting its localised distribution in  
454 development (Kuo et al., 2008). In the current study, we are able to associate TGF- $\beta$   
455 expression also with functional adaptation of the tendon IFM. In addition to tissue  
456 development and homeostasis, TGF- $\beta$ 1 is involved in connective tissue injury and repair with  
457 abnormal expression levels reported in both processes suggesting a pleiotropic mode of  
458 action (Gao et al., 2019). The above may suggest a role for TGF- $\beta$ 1 in tissue development  
459 and homeostasis and that its dysregulation is associated with tissue injury and repair.

460

461 **Outlook**

462 We demonstrate for the first time that functional adaptation in tendon is predominantly reliant  
 463 on adaptation of the metabolically active IFM, which responds to the mechanical  
 464 environment through TGF- $\beta$  signalling, resulting in modulations in ECM turnover and  
 465 composition to fine-tune mechanical properties. Traditionally, the non-collagenous matrix  
 466 phase of connective tissues has received considerably less attention than the fibre phase, with  
 467 regenerative medicine, biomimetics and biomechanics studies all largely focused on  
 468 investigating and recapitulating the organisation and mechanical properties of the collagenous  
 469 fibrous network.

470 Following tendon injury, normal tissue architecture is not recovered, and in particular, the  
 471 cellular IFM is not regenerated. There is great potential gain from understanding the  
 472 convergence of biology underpinning adaptation, function and pathology and here, we  
 473 propose a paradigm shift to consider the metabolically active IFM as a key target for  
 474 regenerative medicine strategies aimed at addressing functional impairment of tendons and  
 475 other connective tissues following disease. Regeneration of the IFM following tendon injury  
 476 could be key for tendon health and low re-injury risk.

477

## 478 **Materials and Methods**

<b>Key Resources Table</b>				
<b>Reagent type (species) or resource</b>	<b>Designation</b>	<b>Source or reference</b>	<b>Identifiers</b>	<b>Additional information</b>
biological sample ( <i>Equus caballus</i> )	Superficial digital flexor tendon and common digital extensor tendon	Equine practices and commercial abattoir		Foetus-2 years old

biological sample ( <i>Equus caballus</i> )	Primary superficial digital flexor tendon tenocytes	Commercial abattoir		P3 from adult specimens
antibody	anti-decorin (mouse IgG)	other		(1:1500), Prof. Caterson, Cardiff University, UK
antibody	anti-proteoglycan 4 (mouse IgG)	other		(1:200), Prof. Caterson, Cardiff University, UK
antibody	anti-fibromodulin (rabbit IgG)	other		(1:400), Prof. Roughley, McGill University, Canada
antibody	anti-tenascin C (mouse IgG)	Santa Cruz Biotechnology	RRID:AB_785991	(1:250)
antibody	anti-elastin (mouse IgG)	Abcam	RRID:AB_2099589	(1:250)
antibody	Zytochem Plus HRP polymer anti-mouse	Zytomed systems	RRID:AB_2868565	(75 µL)
antibody	Zytochem Plus HRP polymer anti-rabbit	Zytomed systems	RRID:AB_2868566	(75 µL)
sequenced-based reagent	<i>Equus caballus</i> TGFBI Accell SMARTpool	Dharmacon, Horizon Discovery	<a href="https://horizondiscovery.com/en/products/tools/Custom-SMARTpool">https://horizondiscovery.com/en/products/tools/Custom-SMARTpool</a>	(1 µM)
sequenced-based reagent	<i>Equus caballus</i> Accell Non-targeting siRNA	Dharmacon, Horizon Discovery	<a href="https://horizondiscovery.com/en/products/tools/Custom-SMARTpool">https://horizondiscovery.com/en/products/tools/Custom-SMARTpool</a>	(1 µM)

peptide, recombinant protein	Recombinant Human TGF-β1	Peprotech	100-21	(10 ng/mL)
commercial assay or kit	FASTIN™ Elastin Assay	Biocolor	<a href="https://www.biocolor.co.uk/product/fastin-elastin-assay/">https://www.biocolor.co.uk/product/fastin-elastin-assay/</a>	
chemical compound, drug	RapiGest SF	Waters	<a href="https://www.waters.com/waters/en_GB/RapiGest-SF-Surfactant/">https://www.waters.com/waters/en_GB/RapiGest-SF-Surfactant/</a>	(0.1% w/v)
software, algorithm	HistoQuest Analysis Software	Tissuegnostics	RRID:SCR_014823	
software, algorithm	Adobe Photoshop CS3	Adobe	RRID:SCR_014199	
software, algorithm	Peaks Studio v8.5	Bioinformatics Solutions	<a href="http://www.bioinformatics.com/peaks-studio">www.bioinformatics.com/peaks-studio</a>	
software, algorithm	Ingenuity Pathway Analysis	Qiagen	RRID:SCR_008653	
software, algorithm	Matrisome	PMID: 2197732	<a href="http://matrisomeproject.mit.edu">http://matrisomeproject.mit.edu</a>	
software, algorithm	Mascot	Matrix Science	RRID:SCR_014322	
software, algorithm	Neopeptide Analyser	PMID: <a href="#">28503667</a>	<a href="https://github.com/PGB-LIV/neo-pep-tool/releases/">https://github.com/PGB-LIV/neo-pep-tool/releases/</a>	
software, algorithm	SigmaPlot	Systat Software Inc	RRID:SCR_003210	
software, algorithm	GProX	PMID: 21602510	RRID:SCR_000273	
other	Chondroitinase ABC from <i>Proteus vulgaris</i>	Merck	C2509	(0.2 U/mL)

other	Hyaluronidase from bovine testes	Merck	H3506	(4800 U/mL)
-------	--	-------	-------	-------------

479

## 480 **Experimental design**

481 Using an equine tendon model, we investigate the process and drivers of functional  
482 adaptation in the SDFT and CDET, two functionally distinct tendons, when tendons transition  
483 from an absence of loading (foetal: mid to end (6 to 9 months) gestation, and 0 days: full-  
484 term foetuses, and foals that did not weight-bear); through to weight-bearing (0-1 month) and  
485 then to an increase in body weight and physical activity (3-6 months; and 1-2 years). We use  
486 a phase-specific approach to characterise each tendon phase independently, by comparing  
487 fascicles (fibre phase) and interfascicular matrix (IFM; matrix phase) mechanical properties,  
488 structure and composition.

489 For this purpose, we used mechanical testing, histological and immunohistochemical analysis  
490 and mass spectrometry analysis following laser capture microdissection. Sample size was  
491 selected based on previous experiments and restricted by sample availability and the cost of  
492 mass spectrometry analysis.

## 493 **Sample collection**

494 Both forelimbs were collected from foetuses and foals aged 0-2 years (n=19) euthanised for  
495 reasons unrelated to this project at a commercial abattoir or equine practices following owner  
496 consent under ethical approval for use of the cadaveric material granted by the Veterinary  
497 Research Ethics Committee, School of Veterinary Science, University of Liverpool  
498 (VREC352). Collected tendons were split in the following age groups: Foetus (between 6 and  
499 9 months of gestation; n=4); 0 days (full-term foetuses (average gestation 11-12 months) and  
500 foals that did not weight-bear; n=4): 0-1 month (n=3); 3-6 months (n=4); 1-2 years (n=4).

501 The SDFT and CDET from one forelimb were dissected and wrapped in phosphate-buffered  
502 saline dampened tissue paper and foil and stored at -80 °C for biomechanical testing. Two 1-2  
503 cm segments from the mid-metacarpal area of the SDFT and CDET of the other forelimb  
504 were dissected, and one fixed in 4% paraformaldehyde for histology and  
505 immunohistochemistry, and the other snap frozen in isopentane and stored at -80 °C for laser  
506 capture microdissection.

### 507 **Biomechanical testing of the fascicles**

508 On the day of testing, samples were defrosted within their tissue paper wrap, then  
509 immediately prepared for testing. Fascicles were dissected from the mid-metacarpal region of  
510 the SDFT and CDET and subjected to a quasi-static test to failure according to Thorpe et al.  
511 (2015) (Thorpe, Godinho, et al., 2015). Briefly, prior to testing, the diameter of each fascicle  
512 was measured along a 1 cm length in the middle of the fascicle with a non-contact laser  
513 micrometre (LSM-501, Mitotuyo, Japan, resolution = 0.5 µm) and the smallest diameter  
514 recorded and used to calculate cross-sectional area (CSA), assuming a circular shape.  
515 Fascicles were loaded in an electrodynamic testing machine (Instron ElectroPuls 1000)  
516 equipped with a 250 N load cell and pneumatic grips (4 bar) coated with rubber and  
517 sandpaper to prevent sample slippage (Thorpe et al., 2012). The distance between the grips  
518 was set to 20 mm and fascicles preloaded to 0.1 N (approx. 2% fascicle failure load) to  
519 remove any slack in the sample. Following preload, the distance between the grips was  
520 recorded as the gauge length, then fascicles preconditioned with 10 loading cycles between 0  
521 and 3% strain (approximately 25% failure strain) using a sine wave at 1 Hz frequency.  
522 Immediately after preconditioning, fascicles were pulled to failure at a strain rate of 5%/s.  
523 Force and extension data were continuously recorded at 100 Hz during both preconditioning  
524 and the quasi-static test to failure. Acquired data were smoothed to reduce noise before



525 calculations with a 3<sup>rd</sup> order Savitzky-Golay low pass filter, with a frame of 15 for the  
526 preconditioning data and 51 for the pull to failure data.

527 Using the preconditioning data, the total percentage hysteresis and stress relaxation were  
528 calculated, between the first and last preconditioning cycle. Failure force, extension, stress,  
529 and strain were calculated from the test to failure, and a continuous modulus calculated  
530 across every 10 data points of each stress strain curve, from which the maximum modulus  
531 value was determined. The point of maximum modulus was defined as the yield point from  
532 which yield stress and yield strain were determined.

### 533 **Biomechanical testing of the IFM**

534 On the day of testing, tendons were defrosted within their tissue paper wrap, and IFM  
535 samples immediately dissected and prepared for biomechanical testing as described  
536 previously by Thorpe et al. (2012) (Thorpe et al., 2012). Briefly, a group of two adjacent  
537 intact fascicles (bound by the IFM) were dissected, after which the opposing end of each  
538 fascicle was cut transversely 10 mm apart, to leave a consistent 10 mm length of intact IFM  
539 that could be tested in shear (Figure 1 – Figure supplement 1c).

540 Utilising the same electrodynamic testing machine and pneumatic grips as described for the  
541 fascicles, the intact end of each fascicle was gripped with a grip to grip distance of 20 mm,  
542 and a pre-load of 0.02 N (approx. 1% IFM failure load) applied. IFM samples were  
543 preconditioned with 10 cycles between 0 and 0.5 mm extension (approx. 25% failure  
544 extension) using a sine wave at 1 Hz frequency, then pulled to failure at a speed of 1 mm/s.  
545 Force and extension data were continuously recorded at 100 Hz during both preconditioning  
546 and the quasi-static test to failure. Acquired data was smoothed to reduce noise before  
547 calculations with a 3<sup>rd</sup> order Savitzky-Golay low pass filter, with a frame of 15 for the  
548 preconditioning data and 51 for the pull to failure data.

549 Total percentage hysteresis and stress relaxation were again calculated between the first and  
550 last preconditioning cycle. Failure force and extension were determined from the quasi-static  
551 pull to failure curve, and a continual stiffness curve was calculated across every 10 data  
552 points of the curve, from which maximum stiffness was determined, and yield force and yield  
553 extension at maximum stiffness reported. Based on previous data demonstrating notable  
554 differences in the toe region of the IFM curve of functionally distinct tendons, the shape of  
555 failure curves was also compared between samples by calculating the amount of IFM  
556 extension at different percentages of IFM failure load (Thorpe, Godinho, et al., 2015).

### 557 **Histology scoring**

558 Paraformaldehyde-fixed paraffin-embedded longitudinal SDFT and CDET segments were  
559 sectioned at 6  $\mu$ m thickness and stained with H&E for histologic examination and scoring  
560 (n=13; 3 from each age group, 4 from 1-2 years age group). The examined histologic  
561 variables are reported in Supplementary File 1 and adapted from Nixon et al. 2008 (Nixon et  
562 al., 2008).

563 For parameters scored by investigators, the sections were blinded and histologic variables  
564 assigned a grade from 0 to 3 by two independent investigators. Weighted Kappa showed  
565 moderate to good agreement in all instances, hence the average of the two scores was used.  
566 Other histologic variables were measured using image analysis (HistoQuest Analysis  
567 software, RRID:SCR\_014823, Tissuegnostics and Adobe Photoshop CS3,  
568 RRID:SCR\_014199) and then assigned a grade from 0 to 3. Cumulative scores for the  
569 fascicle and IFM for each horse were obtained by summing the scores of the fascicle and IFM  
570 variables, respectively, excluding IFM percentage to ensure IFM dimensions were not over-  
571 weighted in final reporting.

### 572 **Immunohistochemistry**

573 Immunohistochemical analysis for DCN, FMOD, PRG4, TNC and ELN was carried out on  
574 paraformaldehyde-fixed paraffin-embedded longitudinal SDFT and CDET sections (6 µm  
575 thickness) (n=12; 3 from each age group) as previously described by Zamboulis et al. (2013)  
576 (Zamboulis et al., 2013). Antigen retrieval was carried out with 0.2 U/mL Chondroitinase  
577 ABC (C2905, Sigma, Merck, Darmstadt, Germany) at 37 °C for two hours for DCN, FMOD,  
578 PRG4, and TNC or with 4800 U/mL hyaluronidase (H3506, Sigma, Merck, Darmstadt,  
579 Germany) at 37 °C for two hours for ELN. Primary antibodies were used at a concentration of  
580 1:1500 for DCN (mouse IgG), 1:400 for FMOD (rabbit IgG), 1:200 for PRG4 (mouse IgG),  
581 1:250 for TNC (mouse IgG, RRID:AB\_785991, Santa Cruz Biotechnology, Dallas, Texas),  
582 and 1:100 for ELN (mouse IgG, RRID:AB\_2099589, Abcam, Cambridge, UK). Antibodies  
583 for DCN and PRG4 were a kind gift from Prof. Caterson, Cardiff University, UK, and the  
584 FMOD antibody was kindly provided by Prof. Roughley, McGill University, Canada. The  
585 secondary antibody incubation was performed with the Zytochem Plus HRP Polymer anti-  
586 rabbit for FMOD and anti-mouse for DCN, PRG4, TNC, and ELN (RRID:AB\_2868566 and  
587 RRID:AB\_2868565, Zytomed Systems, Berlin, Germany). Immunohistochemical staining  
588 was graded from 0 to 3 (low to high) on blinded sections, assessing stained area and staining  
589 intensity for DCN, FMOD, TNC, and ELN. For PRG4, where staining was confined to the  
590 pericellular area, staining intensity was measured using HistoQuest Analysis software  
591 (Tissuegnostics, RRID:SCR\_014823).

## 592 **Quantification of tendon elastin**

593 The elastin content of SDFT and CDET samples from each age group (n=12; 3 from each  
594 age group) was quantified using the FASTIN<sup>TM</sup> Elastin Assay (Biocolor, Carrickfergus,  
595 UK) (Godinho et al., 2017). Briefly, SDFT and CDET tissue was powdered (~15 mg wet  
596 weight) and incubated with 750 µl of 0.25 M oxalic acid at 100 °C for 2 one hour cycles to  
597 extract all soluble a-elastin from the tissue. Preliminary tests showed two extractions were

598 sufficient to solubilise all  $\alpha$ -elastin from developing SDFT and CDET. Following  
599 extraction, samples and standards were processed in duplicate according to the  
600 manufacturer's instructions and their absorbance determined spectrophotometrically at  
601 513 nm (Spectrostar Nano microplate reader, BMG Labtech, Aylesbury, UK). A standard  
602 curve was used to calculate the samples' elastin concentration and elastin was expressed as  
603 a percentage of tendon wet weight.

#### 604 **Laser-capture microdissection**

605 Laser-capture microdissection was used to collect samples from the fascicles and IFM of  
606 SDFT samples from all age groups (n=4 for each age group with the exception of the 0-1  
607 month group where n=3). For this purpose, 12  $\mu$ m transverse cryosections were cut from the  
608 SDFT samples and mounted on steel frame membrane slides (1.4  $\mu$ m PET membrane, Leica  
609 Microsystems, Wetzlar, Germany). Frozen sections were dehydrated in 70% and 100% ice-  
610 cold ethanol, allowed to briefly dry, and regions of fascicle and IFM laser-captured on an  
611 LMD7000 laser microdissection microscope (Leica Microsystems, Wetzlar, Germany) and  
612 collected in LC/MS grade water (FisherScientific, Hampton, New Hampshire). Collected  
613 samples were immediately snap frozen and stored at -80 °C for mass spectrometry analysis.

#### 614 **Mass spectrometry analysis**

615 Mass spectrometry analysis of laser-captured SDFT fascicle and IFM samples was carried out  
616 as previously described by Thorpe et al. (2016) (Thorpe, Peffers, et al., 2016). Samples were  
617 digested for mass spectrometry analysis with incubation in 0.1% (w/v) Rapigest (Waters,  
618 Herts, UK) for 30 min at room temperature followed by 60 min at 60 °C and subsequent  
619 trypsin digestion. LC MS/MS was carried out at the University of Liverpool Centre for  
620 Proteome Research using an Ultimate 3000 Nano system (Dionex/Thermo Fisher Scientific,  
621 Waltham, Massachusetts) for peptide separation coupled online to a Q-Exactive Quadrupole-

622 Orbitrap mass spectrometer (Thermo Scientific, Waltham, Massachusetts) for MS/MS  
623 acquisition. Initial ranging runs on short gradients were carried out to determine the sample  
624 volume to be loaded on the column and subsequently between 1-9  $\mu$ L of sample was loaded  
625 onto the column on a one hour gradient with an inter-sample 30 min blank.

## 626 **Protein identification and label-free quantification**

627 Fascicle and IFM proteins were identified using Peaks® 8.5 PTM software (Bioinformatics  
628 Solutions, Waterloo, Canada), searching against the UniHorse database  
629 (<http://www.uniprot.org/proteomes/>). Search parameters used were: peptide mass tolerance  
630 10 ppm, fragment mass tolerance 0.01 Da, fixed modification carbamidomethylation, variable  
631 modifications methionine oxidation and hydroxylation. Search results for peptide  
632 identification were filtered with a false discovery rate (FDR) of 1%, and for protein  
633 identification with a minimum of 2 unique peptides per protein, and a confidence score  $>20$  (-  
634  $10\lg p > 20$ ). Label-free quantification was also carried out using Peaks® 8.5 PTM software for  
635 the SDFT fascicle and IFM separately. Protein abundances were normalised for collected  
636 laser-capture area and volume loaded onto the mass spectrometry column and differentially  
637 abundant proteins between the age groups in the SDFT fascicle and IFM were identified  
638 using a fold change  $\geq 2$  and  $p < 0.05$  (PEAKS adjusted p values). The mass spectrometry  
639 proteomics data have been deposited to the ProteomeXchange Consortium via the PRIDE  
640 partner repository, with the dataset identifier PXD012169 and 10.6019/PXD012169. With the  
641 IFM showing changes both in its protein composition and mechanical properties during  
642 development and TGFB1 being linked to protein composition, differentially expressed  
643 matrisome proteins identified in the IFM were correlated to TGFB1 whole tendon mRNA  
644 expression and the IFM mechanical properties using the Pearson correlation coefficient  
645 ( $p < 0.05$ ).

## 646 **Gene ontology and network analysis**

647 The dataset of identified proteins in the SDFT fascicles and IFM were classified for cell  
648 compartment association with the Ingenuity Pathway Analysis software (IPA,  
649 RRID:SCR\_008653, Qiagen, Hilden, Germany) and for matrisome categories with The  
650 Matrisome Project database (Hynes & Naba, 2012). Protein pathway analysis for the  
651 differentially abundant proteins between age groups in the SDFT fascicle and IFM was  
652 carried out in IPA. Protein interactions maps were created in IPA allowing for experimental  
653 evidence and highly predicted functional links.

#### 654 **Neopeptide identification**

655 For neopeptide identification, mass spectrometry data was analysed using Mascot server  
656 (Matrix Science, RRID:SCR\_014322) with the search parameters: enzyme semiTrypsin,  
657 peptide mass tolerance 10 ppm, fragment mass tolerance 0.01 Da, charge 2+ and 3+ ions, and  
658 missed cleavages 1. The included modifications were: fixed carbamidomethyl cysteine,  
659 variables oxidation of methionine, proline, and lysine, and the instrument type selected was  
660 electrospray ionization-TRAP (ESI-TRAP). The Mascot-derived ion score was used to  
661 determine true matches ( $p < 0.05$ ), where  $p$  was the probability that an observed match was a  
662 random event. The peptide list was exported and processed with the Neopeptide Analyser, a  
663 software tool for the discovery of neopeptides in proteomic data (Peffer et al., 2017).

664 Obtained neopeptide abundances for each sample were normalised for total peptide  
665 abundance for that protein and sample, and normalised neopeptide abundances were  
666 subsequently summed for each protein and the total neopeptide abundance analysed for  
667 differential abundance across the age groups in the SDFT fascicles and IFM using  $p < 0.05$  and  
668 FDR 5% (ANOVA and Benjamini-Hochberg FDR).

#### 669 **Relative mRNA expression**

670 Laser capture microdissection collects very small amounts of tissue which is not adequate for  
671 mRNA expression analysis and therefore whole tendon was used for the mRNA expression  
672 analysis. RNA extraction from whole SDFT and CDET was carried out followed by reverse  
673 transcription. Quantitative real-time PCR (qRT-PCR) was performed on an ABI7300 system  
674 (Thermo Fisher Scientific Waltham, Massachusetts) using the Takyon ROX SYBR 2X  
675 MasterMix (Eurogentec, Liege, Belgium). qRT-PCR was undertaken using previously  
676 validated gene-specific primers for DCN, FMOD, BGN, COMP, COL1A1, COL1A2,  
677 COL3A1, TGFB1, and GAPDH as a reference gene (Peffer et al., 2013; Taylor et al., 2009)  
678 (Supplementary File 2). Relative expression levels were normalised to GAPDH expression  
679 and calculated with the formula  $E^{-\Delta Ct}$  following primer efficiency calculation.

#### 680 **SiRNA TGFB1 silencing and TGFb1 addition in tenocytes**

681 Tenocytes isolated from young adult SDFT (passage 3, n=4, average age: 5 years old) were  
682 transfected with custom Accell equine TGFB1 siRNA pool and an Accell non-targeting  
683 siRNA (Dharmacon, Horizon Discovery Ltd, Cambridge, UK) for 4 days to silence TGFB1.  
684 Experiments were carried out in the following 24 hours once TGFB1 knockdown was  
685 satisfactory. For TGFB1 stimulation, 10 ng/mL recombinant human TGFB1 (Peprotech,  
686 Cranbury, USA) was added to equine tenocytes for 24 hours, whilst control cells were  
687 incubated in the same media without any additions. qRT-PCR was undertaken as described  
688 above, using previously validated gene-specific primers for TGFB1, BGN, COMP, DCN,  
689 ASPN, FBLN5, COL1A2, COL3A1, and RPS20 as a reference gene (Peffer et al., 2013;  
690 Taylor et al., 2009) (Supplementary File 2).

#### 691 **Statistical analysis**

692 Statistical analysis was carried out in SigmaPlot (RRID:SCR\_003210, Systat Software Inc,  
693 San Jose, California) unless otherwise stated. Details of the n numbers for each experiment

694 and the statistical test used for the analysis of the data are listed in Supplementary File 3.  
695 Heatmaps were designed in GProX (RRID:SCR\_000273) (Rigbolt et al., 2011). The Central  
696 Limit Theorem (CLT) was used to assume normality where  $n > 30$  and where  $n < 30$  normality  
697 was tested using the Shapiro-Wilks test. If data were found not to be normally distributed  
698 their log<sub>10</sub> transformation or ANOVA on Ranks was used for statistical analysis but the  
699 original data was presented in graphs.

700

### 701 **Acknowledgements**

702 This work was funded by the Horserace Betting Levy Board, PRJ/776. We would like to  
703 acknowledge the equine practices that provided samples for this study.

704

### 705 **Author Contributions**

706 DEZ designed and performed experiments, analysed the data, and wrote the manuscript.  
707 CTT assisted with study design, data analysis, and edited the manuscript. YAK assisted  
708 with data collection and analysis. HLB, HRCS, PDC conceived the study, assisted with  
709 data analysis, and edited the manuscript.

710

### 711 **Competing Interests statement**

712 The authors declare that they have no competing interests.

713

### 714 **Data and materials availability**



715 The mass spectrometry proteomics data have been deposited to the ProteomeXchange  
716 Consortium via the PRIDE partner repository, with the dataset identifier PXD012169 and  
717 10.6019/PXD012169.

718

## 719 **References**

- 720 Alexander, R. M. N. (2002). Tendon elasticity and muscle function. *Comparative*  
721 *Biochemistry and Physiology - A Molecular and Integrative Physiology*, 133(4), 1001–  
722 1011. [https://doi.org/10.1016/S1095-6433\(02\)00143-5](https://doi.org/10.1016/S1095-6433(02)00143-5)
- 723 Ansonge, H. L., Adams, S., Birk, D. E., & Soslowky, L. J. (2011). Mechanical,  
724 compositional, and structural properties of the post-natal mouse Achilles tendon. *Annals*  
725 *of Biomedical Engineering*, 39(7), 1904–1913. [https://doi.org/10.1007/s10439-011-](https://doi.org/10.1007/s10439-011-0299-0)  
726 0299-0
- 727 Armiento, A. R., Stoddart, M. J., Alini, M., & Eglin, D. (2018). Biomaterials for articular  
728 cartilage tissue engineering: Learning from biology. *Acta Biomaterialia*, 65, 1–20.  
729 <https://doi.org/10.1016/j.actbio.2017.11.021>
- 730 Batson, E. L., Paramour, R. J., Smith, T. J., Birch, H. L., Patterson-Kane, J. C., & Goodship,  
731 A. E. (2003). Are the material properties and matrix composition of equine flexor and  
732 extensor tendons determined by their functions? *Equine Veterinary Journal*, 35(3), 314–  
733 318. <https://doi.org/10.2746/042516403776148327>
- 734 Biewener, A. A. (1998). Muscle-tendon stresses and elastic energy storage during locomotion  
735 in the horse. *Comparative Biochemistry and Physiology - B Biochemistry and Molecular*  
736 *Biology*, 120(1), 73–87. [https://doi.org/10.1016/S0305-0491\(98\)00024-8](https://doi.org/10.1016/S0305-0491(98)00024-8)
- 737 Birch, H. L. (2007). Tendon matrix composition and turnover in relation to functional  
738 requirements. *International Journal of Experimental Pathology*, 88(4), 241–248.  
739 <https://doi.org/10.1111/j.1365-2613.2007.00552.x>

740 Birch, H. L., Worboys, S., Eissa, S., Jackson, B., Strassburg, S., & Clegg, P. D. (2008).  
741 Matrix metabolism rate differs in functionally distinct tendons. *Matrix Biology*, 27(3),  
742 182–189. <https://doi.org/10.1016/j.matbio.2007.10.004>

743 Cherdchutham, W., Becker, C. K., Spek, E. R., Voorhout, W. E., & Van Weeren, P. R.  
744 (2001). Effects of exercise on the diameter of collagen fibrils in the central core and  
745 periphery of the superficial digital flexor tendon in foals. *American Journal of*  
746 *Veterinary Research*, 62(10), 1563–1570. <https://doi.org/10.2460/ajvr.2001.62.1563>

747 Cherdchutham, W., Meershoek, L. S., Weeren, P. R. Van, & Barneveld, A. (2001). Effects of  
748 exercise on biomechanical properties of the superficial digital flexor tendon in foals.  
749 *American Journal of Veterinary Research*, 62(12), 1859–1864. [https://avmajournals-](https://avmajournals-avma-org.proxy1.cl.msu.edu/doi/pdf/10.2460/ajvr.2001.62.1859)  
750 [avma-org.proxy1.cl.msu.edu/doi/pdf/10.2460/ajvr.2001.62.1859](https://avmajournals-avma-org.proxy1.cl.msu.edu/doi/pdf/10.2460/ajvr.2001.62.1859)

751 Choi, R. K., Smith, M., Clarke, E., & Little, C. (2018). Cellular, matrix, and mechano-  
752 biological differences in load-bearing versus positional tendons throughout development  
753 and aging: a narrative review. *Connective Tissue Research*, 59(5), 483–494.  
754 <https://doi.org/10.1080/03008207.2018.1504929>

755 Choi, R. K., Smith, M. M., Smith, S., Little, C. B., & Clarke, E. C. (2019). Functionally  
756 distinct tendons have different biomechanical, biochemical and histological responses to  
757 in vitro unloading. *Journal of Biomechanics*, 95, 109321.  
758 <https://doi.org/10.1016/j.jbiomech.2019.109321>

759 Freedman, B. R., Bade, N. D., Riggin, C. N., Zhang, S., Haines, P. G., Ong, K. L., & Janmey,  
760 P. A. (2015). The (dys)functional extracellular matrix. *Biochimica et Biophysica Acta -*  
761 *Molecular Cell Research*, 1853(11), 3153–3164.  
762 <https://doi.org/10.1016/j.bbamcr.2015.04.015>

763 Gao, F., Li, C., Zhou, J., Shen, X., Hu, B., Lu, M., Liu, Y., Zhang, B., Fang, Y., & Liu, Y.  
764 (2019). Progress on relationship between transforming growth factor-beta1 and

765           tendinopathy. *China Journal of Orthopaedics and Traumatology*, 32(4), 377–382.

766 Gardner, K., Arnoczky, S. P., Caballero, O., & Lavagnino, M. (2008). The effect of stress-  
767           deprivation and cyclic loading on the TIMP/MMP ratio in tendon cells: An in vitro  
768           experimental study. *Disability and Rehabilitation*, 30(20–22), 1523–1529.  
769           <https://doi.org/10.1080/09638280701785395>

770 Godinho, M. S. C., Thorpe, C. T., Greenwald, S. E., & Screen, H. R. C. (2017). Elastin is  
771           Localised to the Interfascicular Matrix of Energy Storing Tendons and Becomes  
772           Increasingly Disorganised With Ageing. *Scientific Reports*, 7(1), 1–11.  
773           <https://doi.org/10.1038/s41598-017-09995-4>

774 Heinemeier, K. M., Schjerling, P., Heinemeier, J., Magnusson, S. P., & Kjaer, M. (2013).  
775           *Lack of tissue renewal in human adult Achilles tendon is revealed by nuclear bomb 14C*  
776           (pp. 2074–2079).

777 Hynes, R. O., & Naba, A. (2012). Overview of the matrisome-An inventory of extracellular  
778           matrix constituents and functions. *Cold Spring Harbor Perspectives in Biology*, 4(1), 1–  
779           16. <https://doi.org/10.1101/cshperspect.a004903>

780 Kalson, N. S., Holmes, D. F., Herchenhan, A., Lu, Y., Starborg, T., & Kadler, K. E. (2011).  
781           Slow stretching that mimics embryonic growth rate stimulates structural and mechanical  
782           development of tendon-like tissue in vitro. *Developmental Dynamics*, 240(11), 2520–  
783           2528. <https://doi.org/10.1002/dvdy.22760>

784 Kohrs, R. T., Zhao, C., Sun, Y. L., Jay, G. D., Zhang, L., Warman, M. L., An, K. N., &  
785           Amadio, P. C. (2011). Tendon fascicle gliding in wild type, heterozygous, and lubricin  
786           knockout mice. *Journal of Orthopaedic Research*, 29(3), 384–389.  
787           <https://doi.org/10.1002/jor.21247>

788 Kostrominova, T. Y., & Brooks, S. V. (2013). Age-related changes in structure and  
789           extracellular matrix protein expression levels in rat tendons. *Age*, 35(6), 2203–2214.

790 <https://doi.org/10.1007/s11357-013-9514-2>

791 Kuo, C., Petersen, B., & Tuan, R. (2008). Spatiotemporal protein distribution of TGF- $\beta$ 's,  
792 their receptors, and extracellular matrix molecules during embryonic tendon  
793 development. *Developmental Dynamics*, 237(5), 1477–1489.  
794 <https://doi.org/10.1002/dvdy.21547>.Spatiotemporal

795 Maeda, T., Sakabe, T., Sunaga, A., Sakai, K., Rivera, A. L., Keene, D. R., Sasaki, T.,  
796 Stavnezer, E., Iannotti, J., Schweitzer, R., Ilic, D., Baskaran, H., & Sakai, T. (2011).  
797 Conversion of mechanical force into TGF- $\beta$ -mediated biochemical signals. *Current*  
798 *Biology*, 21(11), 933–941. <https://doi.org/10.1016/j.cortex.2009.08.003>.Predictive

799 Magnusson, S. P., & Kjaer, M. (2019). The impact of loading, unloading, ageing and injury  
800 on the human tendon. *Journal of Physiology*, 597(5), 1283–1298.  
801 <https://doi.org/10.1113/JP275450>

802 Marturano, J. E., Arena, J. D., Schiller, Z. A., Georgakoudi, I., & Kuo, C. K. (2013).  
803 Characterization of mechanical and biochemical properties of developing embryonic  
804 tendon. *Proceedings of the National Academy of Sciences of the United States of*  
805 *America*, 110(16), 6370–6375. <https://doi.org/10.1073/pnas.1300135110>

806 Mendias, C. L., Gumucio, J. P., & Lynch, E. B. (2012). Mechanical loading and TGF- $\beta$   
807 change the expression of multiple miRNAs in tendon fibroblasts. *Journal of Applied*  
808 *Physiology*, 113(1), 56–62. <https://doi.org/10.1152/jappphysiol.00301.2012>

809 Nixon, A. J., Dahlgren, L. A., Haupt, J. L., Yeager, A. E., & Ward, D. L. (2008). Effect of  
810 adipose-derived nucleated cell fractions on tendon repair in horses with collagenase-  
811 induced tendinitis. *American Journal of Veterinary Research*, 69(7).

812 Pan, X. S., Li, J., Brown, E. B., & Kuo, C. K. (2018). Embryo movements regulate tendon  
813 mechanical property development. *Philosophical Transactions of the Royal Society B:*  
814 *Biological Sciences*, 373(1759). <https://doi.org/10.1098/rstb.2017.0325>

815 Patterson-Kane, J. C., & Rich, T. (2014). Achilles tendon injuries in elite athletes: Lessons in  
816 pathophysiology from their equine Counterparts. *ILAR Journal*, 55(1), 86–99.  
817 <https://doi.org/10.1093/ilar/ilu004>

818 Peffers, M. J., Jones, A. R., McCabe, A., & Anderson, J. (2017). Neopeptide Analyser: A  
819 software tool for neopeptide discovery in proteomics data. *Wellcome Open Research*,  
820 2(May), 1–9. <https://doi.org/10.12688/wellcomeopenres.11275.1>

821 Peffers, M. J., Liu, X., & Clegg, P. D. (2013). Transcriptomic signatures in cartilage ageing.  
822 *Arthritis Research and Therapy*, 15(4), R98. <https://doi.org/10.1186/ar4278>

823 Potter, R. M., Huynh, R. T., Volper, B. D., Arthur, K. A., D'Lugos, A. C., Sørensen, M. A.,  
824 Peter Magnusson, S., Dickinson, J. M., Hale, T. M., & Carroll, C. C. (2017). Impact of  
825 TGF- $\beta$  inhibition during acute exercise on achilles tendon extracellular matrix.  
826 *American Journal of Physiology - Regulatory Integrative and Comparative Physiology*,  
827 312(1), R157–R164. <https://doi.org/10.1152/ajpregu.00439.2016>

828 Rigbolt, K. T. G., Vanselow, J. T., & Blagoev, B. (2011). GProX, a user-friendly platform for  
829 bioinformatics analysis and visualization of quantitative proteomics data. *Molecular and*  
830 *Cellular Proteomics*, 10(8), 1–10. <https://doi.org/10.1074/mcp.O110.007450>

831 Ritty, T. M., Ditsios, K., & Starcher, B. C. (2002). Distribution of the elastic fiber and  
832 associated proteins in flexor tendon reflects function. *Anatomical Record*, 268(4), 430–  
833 440. <https://doi.org/10.1002/ar.10175>

834 Robbins, J. R., Evanko, S. P., & Vogel, K. G. (1997). Mechanical loading and TGF- $\beta$   
835 regulate proteoglycan synthesis in tendon. *Archives of Biochemistry and Biophysics*,  
836 342(2), 203–211. <https://doi.org/10.1006/abbi.1997.0102>

837 Russo, V., Mauro, A., Martelli, A., Di Giacinto, O., Di Marcantonio, L., Nardinocchi, D.,  
838 Berardinelli, P., & Barboni, B. (2015). Cellular and molecular maturation in fetal and  
839 adult ovine calcaneal tendons. *Journal of Anatomy*, 226(2), 126–142.

840 <https://doi.org/10.1111/joa.12269>

841 Sensini, A., Gualandi, C., Focarete, M., Belcari, J., Zucchelli, A., Boyle, L., Reilly, G., Kao,  
842 A., Tozzi, G., & Cristofolini, L. (2019). Multiscale hierarchical bioresorbable scaffolds  
843 for the regeneration of tendons and ligaments. *Biofabrication*, *11*(3), 035026.

844 Simpson, D., Choi, H., Wang, D., Prescott, M., Pitsillides, A. A., Dudhia, J., Clegg, P. D.,  
845 Ping, P., & Thorpe, C. T. (2020). Heterogeneity of proteome dynamics between  
846 connective tissue phases of adult tendon. *ELife*, *9*, 1–29.  
847 <https://doi.org/10.7554/eLife.55262>

848 Spiesz, E. M., Thorpe, C. T., Chaudhry, S., Riley, G. P., Birch, H. L., Clegg, P. D., & Screen,  
849 H. R. C. (2015). Tendon extracellular matrix damage, degradation and inflammation in  
850 response to in vitro overload exercise. *Journal of Orthopaedic Research*, *33*(6), 889–  
851 897. <https://doi.org/10.1002/jor.22879>

852 Stanley, R. L., Edwards, L. J., Goodship, A. E., Firth, E. C., & Patterson-Kane, J. C. (2008).  
853 Effects of exercise on tenocyte cellularity and tenocyte nuclear morphology in immature  
854 and mature equine digital tendons. *Equine Veterinary Journal*, *40*(2), 141–146.  
855 <https://doi.org/10.2746/042516408X266097>

856 Subramanian, A., Kanzaki, L. F., Galloway, J. L., & Schilling, T. F. (2018). Mechanical force  
857 regulates tendon extracellular matrix organization and tenocyte morphogenesis through  
858 TGFbeta signaling. *ELife*, *7*, 1–24. <https://doi.org/10.7554/eLife.38069>

859 Subramanian, A., & Schilling, T. F. (2014). Thrombospondin-4 controls matrix assembly  
860 during development and repair of myotendinous junctions. *ELife*, *2014*(3), 1–21.  
861 <https://doi.org/10.7554/eLife.02372>

862 Taye, N., Karoulias, S. Z., & Hubmacher, D. (2020). The “other” 15–40%: The Role of Non-  
863 Collagenous Extracellular Matrix Proteins and Minor Collagens in Tendon. *Journal of*  
864 *Orthopaedic Research*, *38*(1), 23–35. <https://doi.org/10.1002/jor.24440>

865 Taylor, S. E., Vaughan-Thomas, A., Clements, D. N., Pinchbeck, G., MacRory, L. C., Smith,  
866 R. K., & Clegg, P. D. (2009). Gene expression markers of tendon fibroblasts in normal  
867 and diseased tissue compared to monolayer and three dimensional culture systems. *BMC*  
868 *Musculoskeletal Disorders*, *10*, 1–10. <https://doi.org/10.1186/1471-2474-10-27>

869 Thorpe, C. T., Chaudhry, S., Lei, I. I., Varone, A., Riley, G. P., Birch, H. L., Clegg, P. D., &  
870 Screen, H. R. C. (2015). Tendon overload results in alterations in cell shape and  
871 increased markers of inflammation and matrix degradation. *Scandinavian Journal of*  
872 *Medicine and Science in Sports*, *25*(4), e381–e391. <https://doi.org/10.1111/sms.12333>

873 Thorpe, C. T., Godinho, M. S. C., Riley, G. P., Birch, H. L., Clegg, P. D., & Screen, H. R. C.  
874 (2015). The interfascicular matrix enables fascicle sliding and recovery in tendon, and  
875 behaves more elastically in energy storing tendons. *Journal of the Mechanical Behavior*  
876 *of Biomedical Materials*, *52*, 85–94. <https://doi.org/10.1016/j.jmbbm.2015.04.009>

877 Thorpe, C. T., Karunaseelan, K. J., Ng Chieng Hin, J., Riley, G. P., Birch, H. L., Clegg, P.  
878 D., & Screen, H. R. C. (2016). Distribution of proteins within different compartments of  
879 tendon varies according to tendon type. *Journal of Anatomy*, *229*(3), 450–458.  
880 <https://doi.org/10.1111/joa.12485>

881 Thorpe, C. T., Peffers, M. J., Simpson, D., Halliwell, E., Screen, H. R. C., & Clegg, P. D.  
882 (2016). Anatomical heterogeneity of tendon: Fascicular and interfascicular tendon  
883 compartments have distinct proteomic composition. *Scientific Reports*, *6*(February), 1–  
884 12. <https://doi.org/10.1038/srep20455>

885 Thorpe, C. T., Riley, G. P., Birch, H. L., Clegg, P. D., & Screen, H. R. C. (2016). Fascicles  
886 and the interfascicular matrix show adaptation for fatigue resistance in energy storing  
887 tendons. *Acta Biomaterialia*, *42*, 308–315. <https://doi.org/10.1016/j.actbio.2016.06.012>

888 Thorpe, C. T., & Screen, H. R. C. (2016). Tendon structure and composition. In *Advances in*  
889 *Experimental Medicine and Biology* (Vol. 920). <https://doi.org/10.1007/978-3-319->

890 33943-6

891 Thorpe, C. T., Streeter, I., Pinchbeck, G. L., Goodship, A. E., Clegg, P. D., & Birch, H. L.  
892 (2010). Aspartic acid racemization and collagen degradation markers reveal an  
893 accumulation of damage in tendon collagen that is enhanced with aging. *Journal of*  
894 *Biological Chemistry*, 285(21), 15674–15681. <https://doi.org/10.1074/jbc.M109.077503>

895 Thorpe, C. T., Udeze, C. P., Birch, H. L., Clegg, P. D., & Screen, H. R. C. (2012).  
896 Specialization of Tendon Mechanical Properties Results From Interfascicular  
897 Differences. *Journal of The Royal Society Interface*, 9(76), 3108–3117.

898 Thorpe, C. T., Udeze, C. P., Birch, H. L., Clegg, P. D., & Screen, H. R. C. (2013). Capacity  
899 for sliding between tendon fascicles decreases with ageing in injury prone equine  
900 tendons: A possible mechanism for age-related tendinopathy? *European Cells and*  
901 *Materials*, 25(0), 48–60.

902 Watts, A. E., Millar, N. L., Platt, J., Kitson, S. M., Akbar, M., Rech, R., Griffin, J., Pool, R.,  
903 Hughes, T., McInnes, I. B., & Gilchrist, D. S. (2017). MicroRNA29a Treatment  
904 Improves Early Tendon Injury. *Molecular Therapy*, 25(10), 2415–2426.  
905 <https://doi.org/10.1016/j.ymthe.2017.07.015>

906 Zamboulis, D. E., Senior, J. M., Clegg, P. D., Gallagher, J. A., Carter, S. D., & Milner, P. I.  
907 (2013). Distribution of purinergic P2X receptors in the equine digit, cervical spinal cord  
908 and dorsal root ganglia. *Purinergic Signalling*, 9(3), 383–393.  
909 <https://doi.org/10.1007/s11302-013-9356-5>

910

911



912 **Supplementary data**

913 **Figure 1 – Figure supplement 1.** SDFT and CDET in the equine forelimb, tendon structure,  
914 and schematic showing procedure for biomechanical testing.

915 **Figure 3 – Figure supplement 1.** Scoring of histologic variables for the IFM and fascicle in  
916 the SDFT and CDET through postnatal development.

917 **Figure 4 – Figure supplement 1.** Scoring of ELN staining for the IFM and fascicle in the  
918 SDFT and CDET through postnatal development.

919 **Figure 5 – Figure supplement 1.** Classification of SDFT IFM and fascicle identified  
920 proteins and differentially abundant proteins according to their associated location.

921 **Figure 5 – Figure supplement 2.** Relative mRNA expression of major ECM genes in whole  
922 tissue SDFT and CDET through postnatal development.

923 **Supplementary File 1.** Histologic variables used in the H&E scoring of the SDFT and  
924 CDET sections and the analysis method and reporting criteria adopted.

925 **Supplementary File 2.** Gene primer sequences used in relative mRNA expression analysis.

926 **Supplementary File 3.** Samples used for analysis along with statistical test used for analysis.

927 **Supplementary File 4.** Collagens and proteoglycans identified in SDFT IFM and fascicle.

928 **Supplementary File 5.** Correlation analysis of IFM protein abundance and mechanical  
929 properties across development.

930 **Supplementary File 6.** Correlation analysis of TGFB1 whole tendon mRNA expression and  
931 IFM protein abundance across development.

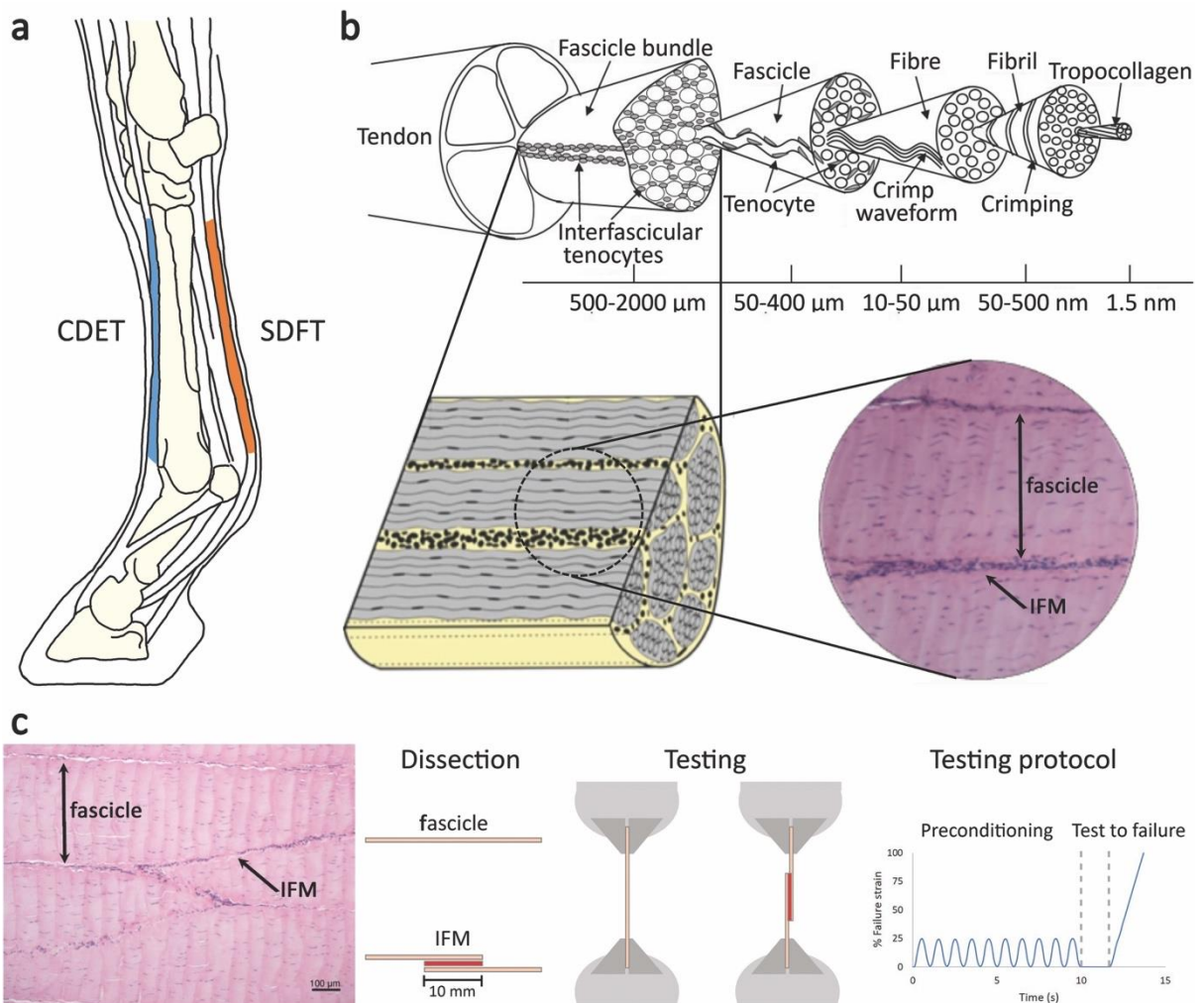
932 **Figure 1 and 2 – Source Data 1.** Fascicle and IFM mechanical properties.

933 **Table 1 and 2 – Source Data 2.** IFM and fascicle matrix proteins intensity.

934

935

936



937  
938

**Figure 1 – Figure supplement 1. SDFT and CDET in the equine forelimb, tendon**

939

**structure, and schematic showing procedure for biomechanical testing.** (a) Schematic of

940

the equine forelimb with the CDET and SDFT highlighted. (b) Tendon structure (partially

941

reproduced from Figure 1, Spiesz et al. 2015, *Journal of Orthopaedic Research*, published

942

under the Creative Commons Attribution 4.0 International Public License (CC BY 4.0;

943

<https://creativecommons.org/licenses/by/4.0/>). (c) H&E section of fascicle and IFM and

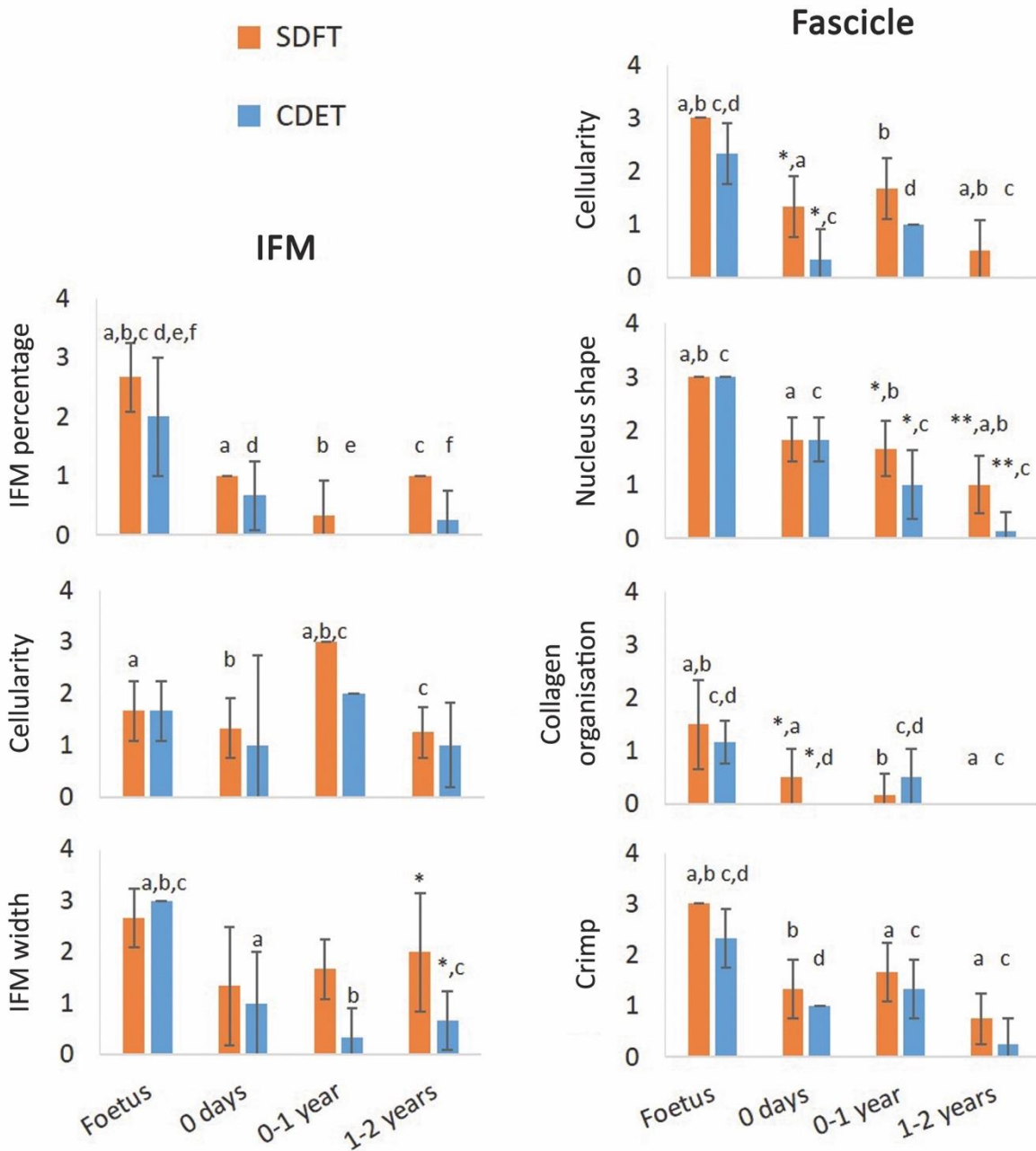
944

schematic of fascicle and IFM dissection and biomechanical testing.

945

946

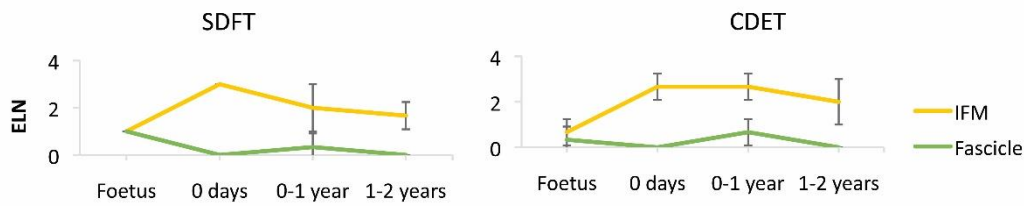
IFM	Scoring	Fascicle	Scoring
Percentage of IFM	0 – 3, lower to higher	Cellularity	0 – 3, fewer - more
IFM width	0 – 3, smaller to larger	Nucleus shape	0 – 3, elongated to rounded
Cellularity	0 – 3, fewer - more	Organisation of collagen fibres	0 – 3, linear to non-linear
		Crimp angle	0 – 3, smaller to larger



947  
948 **Figure 3 – Figure supplement 1. Scoring of histologic variables for the IFM and fascicle**  
949 **in the SDFT and CDET through postnatal development. \* significant difference between**  
950 **tendons, a-f significant difference between age groups. Error bars depict standard deviation.**

951

952



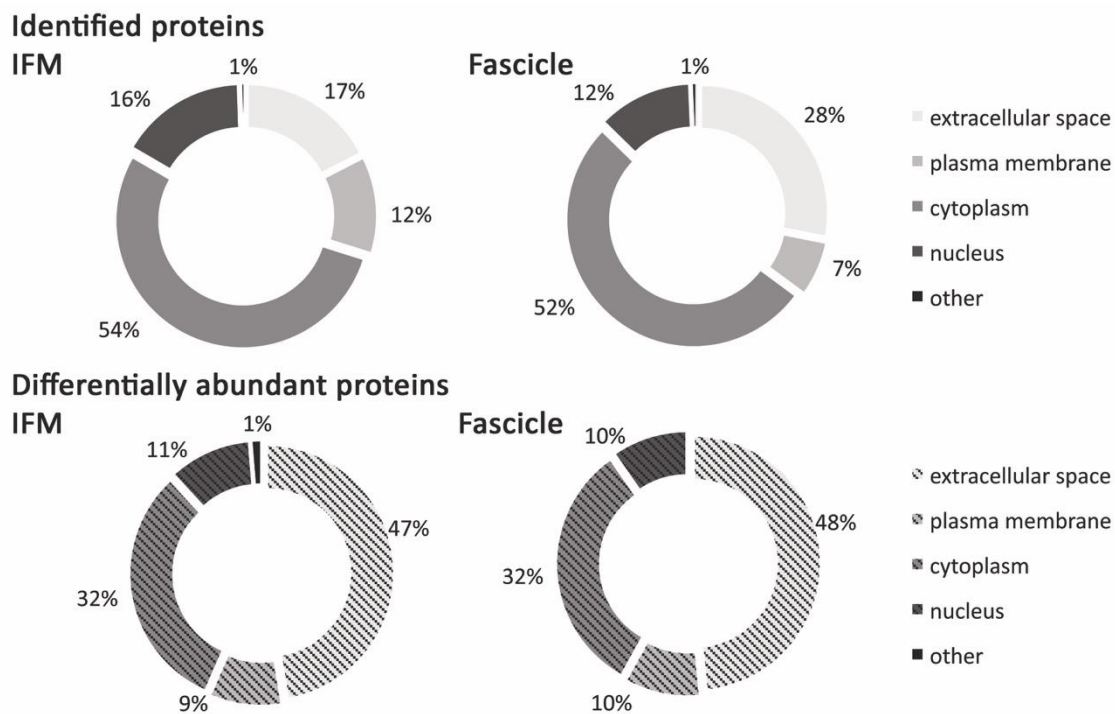
953

954 **Figure 4 – Figure supplement 1. Scoring of ELN staining for the IFM and fascicle in the**

955 **SDFT and CDET through postnatal development. Error bars depict standard deviation.**

956

957



958

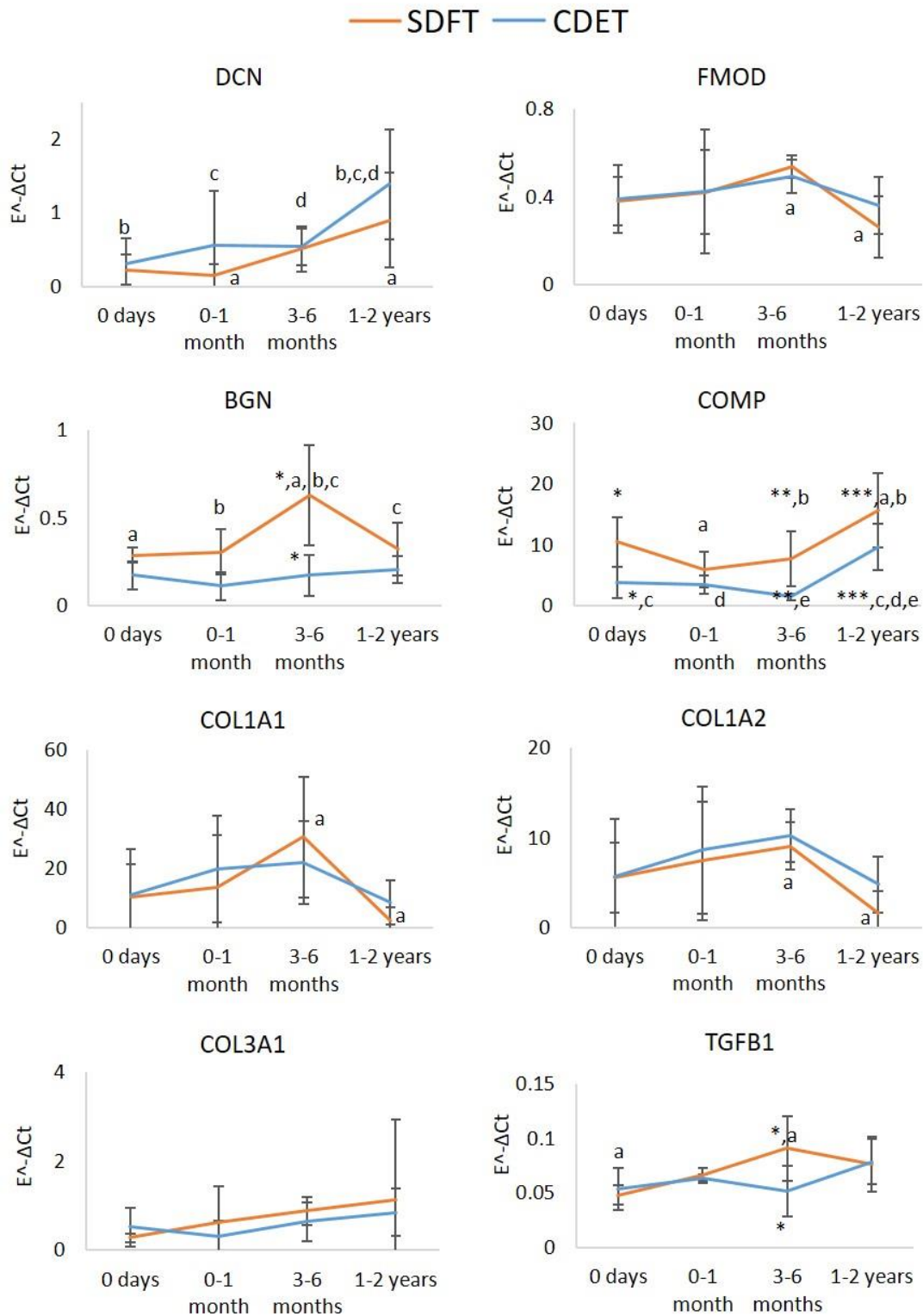
959 **Figure 5 – Figure supplement 1. Classification of SDFT IFM and fascicle identified**

960 **proteins and differentially abundant proteins ( $p < 0.05$ , fold change  $\geq 2$ ) according to their**

961 **associated location.**

962

963



964

965 **Figure 5 – Figure supplement 2. Relative mRNA expression of major ECM genes in**  
 966 **whole tissue SDFT and CDET through postnatal development. \* significant difference**  
 967 **between tendons, a-e significant difference between age groups. Error bars depict standard**  
 968 **deviation.**